Storm-time Disturbed Electric Field Influence in the Strong Sporadic E-layers Occurrence over Boa Vista, a low latitude Brazilian Region

Resende Laysa Cristina Araujo[1], Jiankui Shi[2], Denardini Clezio Marcos[3], Nogueira Paulo Alexandre Bronzato[4], Batista Inez S.[3], Arras Christina[5], Andrioli Vania Fatima[6], Moro Juliano[7], Da Silva Ligia Alves[8], Carrasco Alexander Jose[9], Barbosa Neto Paulo França[3], Wang Chi[10], and Zhengkuan Liu[11]

[1]National Institute for Space Research/China-Brazil Joint Laboratory of Space Weather
[2]State Key Laboratory of Space Weather, China Academy of Science, CAS
[3]National Institute for Space Research
[4]Federal Institute of Education, Science and Technology of Sao Paulo
[5]GFZ Potsdam
[6]National Institute for Space Research - INPE
[7]Southern Regional Space Research Center - CRS/COCRE/INPE
[8]National Institute for Space Research (INPE) / China-Brazil Joint Laboratory for Space Weather
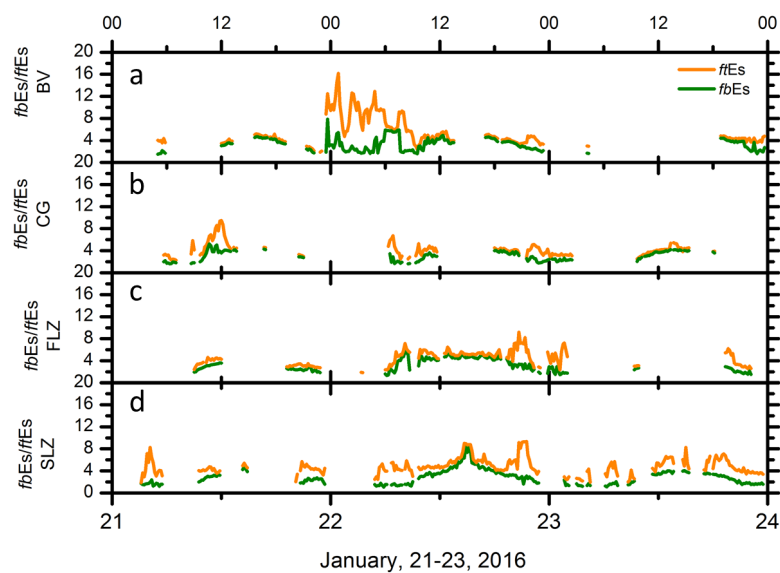[9]Universidad de los Andes
[10]National Space Science Center, Chinese Academy of Sciences
[11]State Key Laboratory of Space Weather, National Space Science Center (NSSC), Chinese Academy of Sciences

November 16, 2022

Abstract

The formation of strong sporadic E-layers (Es) is frequently observed during the recovery phase of the magnetic storms over Boa Vista (BV, 2.8°N, 60.7°W), a low latitude region over the Brazilian sector. To provide some explanation for this behavior, we investigated in details the ionospheric response to the disturbed electric fields in these atypical Es layers appearance during the magnetic storm of 21-22 January 2016. The analysis was based on F region and Es layers ionospheric parameters obtained from digisonde, as well as on the Total Electron Content (TEC) obtained from Global Navigation SatelliteSystem (GNSS). Furthermore, a theoretical model for the E region named MIRE is used to simulate the Es layers development. Such simulation takes into account the E region winds and electric fields. The results show that the storm time electric field is enough to drive the strong Es layers development. Moreover, it is seen that the intensification of the Es layers is related to the inhibition of the F-region pre-reversal enhancement of the vertical drift due to a westward electric field during the disturbance dynamo effect. Finally, the combined results from the model and observational data seemed to contribute significantly to advance our understanding of the role of the electric fields in the Es layer formation.
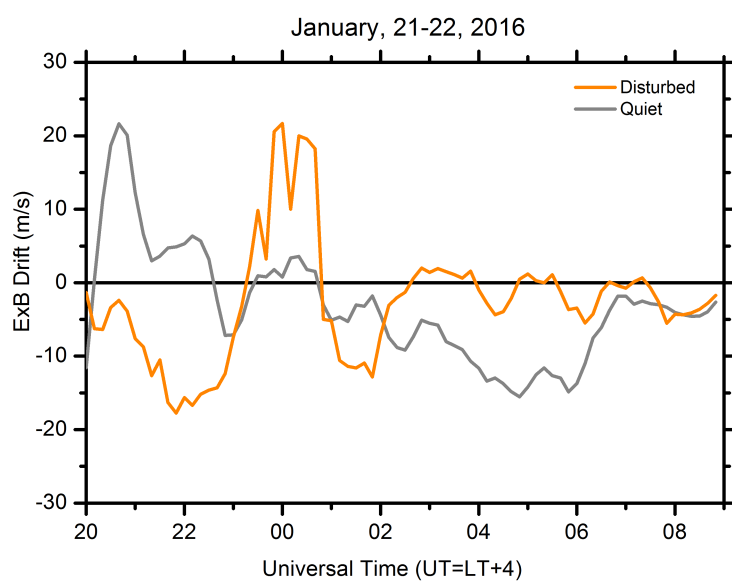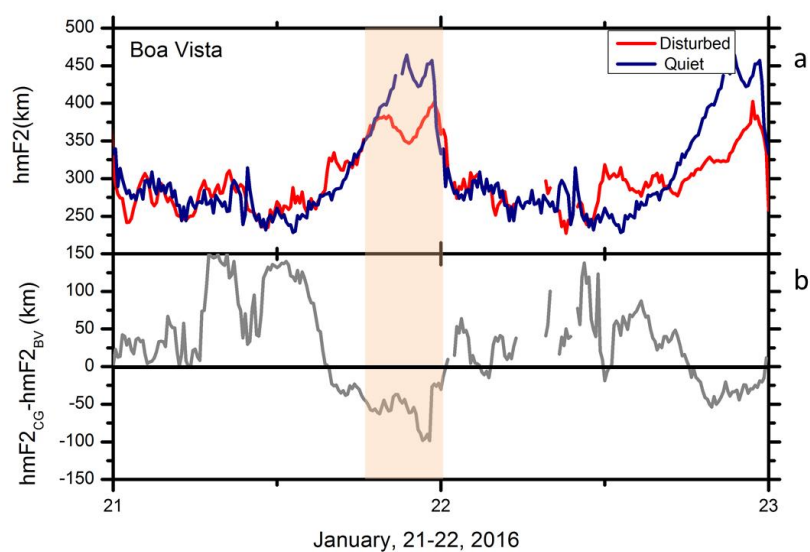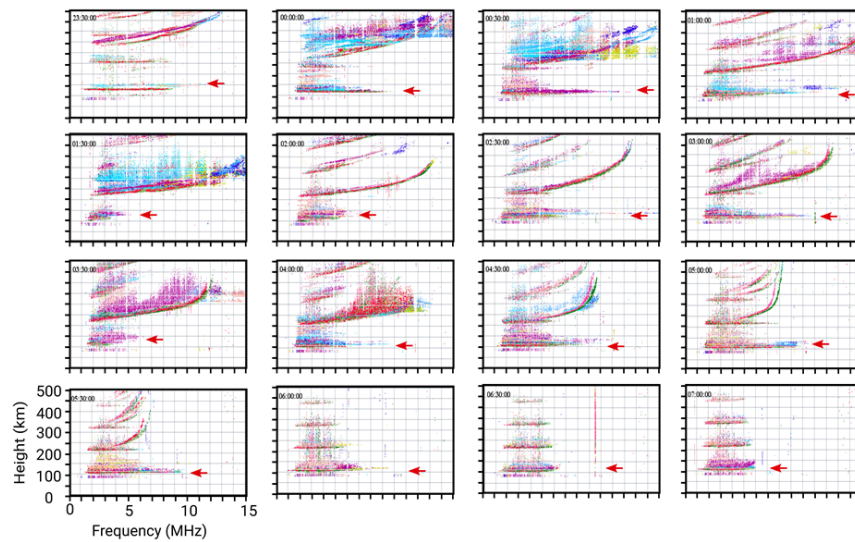
January, 18, 2016
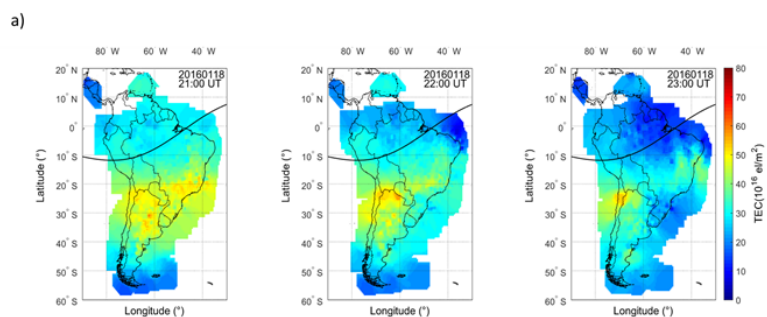
January, 21, 2016
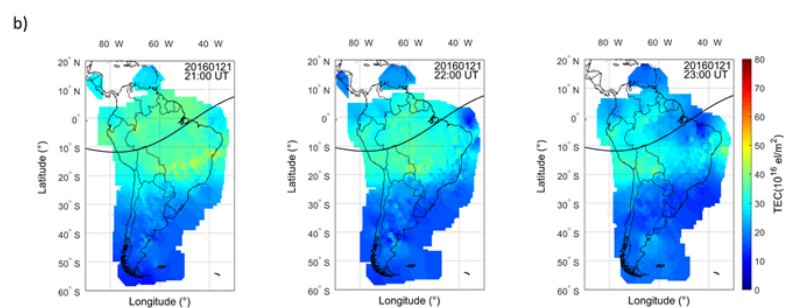
Storm-time Disturbed Electric Field Influence in the Strong Sporadic E-layers Occurrence over Boa Vista, a low latitude Brazilian Region

L. C. A. Resende[1,2*], S. Jiankui[1], C. M. Denardini[2], P. A. B. Nogueira[3], I. S. Batista[2], C. Arras[4], V. F. Andrioli [1,2], J. Moro[1,6], L. Silva[1,2], A. J. Carrasco[5], P. F. Barbosa[2,7], C. Wang[1], Z. Liu[1]

[1]State Key Laboratory of Space Weather, Beijing, China.

[2]National Institute for Space Research – INPE, São José dos Campos-SP, Brazil.

[3] Federal Institute of Education, Science and Technology of São Paulo, Jacarei - SP, Brazil

[4]Helmholtz Centre Potsdam, German Research Centre for Geosciences (GFZ), Department 1: Geodesy and Remote Sensing, Potsdam, Germany

[5] University of Los Andes, Mérida, Venezuela

[6]Southern Regional Space Research Center – CRS/COCRE/INPE, Santa Maria-RS, Brazil.

[7]Salesian University Center São Paulo, Campus São Joaquim, Lorena-SP, Brazil

Corresponding author: Laysa Resende (laysa.resende@inpe.br; laysa.resende@gmail.com)

Key Points:

- Anomalous Sporadic E layers that occurred in a low latitude Brazilian region, Boa Vista.

- The influence of the disturbed dynamo electric field in the strong Es layers in Boa Vista.

- The simulations allowed analyzing the electric field magnitude that caused the Es layer intensification.

Abstract

The formation of strong sporadic E-layers (Es) is frequently observed during the recovery phase of the magnetic storms over Boa Vista (BV, 2.8°N, 60.7°W), a low latitude region over the Brazilian sector. To provide some explanation for this behavior, we investigated in details the ionospheric response to the disturbed electric fields in these atypical Es layers appearance during the magnetic storm of 21-22 January 2016. The analysis was based on F region and Es layers ionospheric parameters obtained from digisonde, as well as on the Total Electron Content (TEC) obtained from Global Navigation Satellite System (GNSS). Furthermore, a theoretical model for the E region named MIRE is used to simulate the Es layers development. Such simulation takes into account the E region winds and electric fields. The results show that the storm time electric field is enough to drive the strong Es layers development. Moreover, it is seen that the intensification of the Es layers is related to the inhibition of the F-region pre-reversal enhancement of the vertical drift due to a westward electric field during the disturbance dynamo effect. Finally, the combined results from the model and observational data seemed to contribute significantly to advance our understanding of the role of the electric fields in the Es layer formation.

1 Introduction

Sporadic E (Es) layers are denser and thin layers which are mainly formed by the wind-shear mechanism in low/mid-latitudes [*Whitehead, 1961; Mathews, 1998; Haldoupis, 2011*]. The metallic ions of meteoric origin are accumulated at the null points of the winds causing density enhancement at E-region heights. Although these layers are named sporadic, they could be considered as permanent layers due to its frequent observation and the long lifetime of the metallic ions, such as Fe^+, Mg^+, K^+, Ca^+ and Na^+ [*Kopp, 1997*]. The Es layer characteristics were addressed by several authors showing that their intensity and locations are controlled generally by the tidal wind atmospheric dynamics [*Prassad et al., 2012; Pignalberi et al., 2014; Resende et al. 2017a*], and in some cases by the electric field [*Abdu et al., 2014, Resende et al. 2017b, Moro et al., 2017*].

Close to the geomagnetic equator the influence of the electric fields in the Es layer formation becomes more important since the wind shear is not the favorable mechanism in these regions. *Dagar et al. [1977]* showed that a zonal electric field component smaller than 2 mV/m could influence the Es layers formation in regions around the magnetic equator. In addition, it is well established that at equatorial regions the Es trace commonly observed on daytime ionograms is due to irregularities in the E-layers, and not a reflection from a denser layer. In fact, the diffuse and non-blanketing layer, which is classified as q-type Es or Es_q, is the manifestation of the gradient drift instability in ionograms (Type II irregularities) due to the Equatorial Electrojet Current (EEJ) [*Abdu et al., 1996; Resende et al., 2016*].

Abdu et al. [2009b] investigated the relationship between the Es layers occurrence/disruption at a low latitude location (Fortaleza) and the evening pre-reversal enhancement (PRE) in the vertical drift (or electric field) at the dip equator. They found that depending on the PRE amplitude a disruption or intensification of the Es layers could occur. *Carrasco et al. [2007]* developed a numerical model for the E region and was able to simulate that an upward (positive) vertical electric field is capable of disrupting an ongoing sporadic

72 layer, whereas a downward (negative) electric field favors its intensification or even formation.
73 *Resende et al. [2016]* used the same model to analyze the electric field effect in Es layer during
74 quiet time. They found that the electric field vertical component of the EEJ interrupts the dense
75 layer occurrence. Also, the results confirmed that the winds are the main factor to form Es layer
76 at low latitudes. *Moro et al. [2017]* used this same model to analyze the electric field influence
77 in the equatorial Es layer formation during the magnetic storm that occurred in November 2004.
78 They verified that the vertical electric fields of the EEJ irregularity suffer intense changes,
79 disrupting the Es_q layers. Notice, however, that the electric field effect in the Es layer
80 development at low latitudes is still poorly understood. In fact, to the best of our knowledge,
81 there are no studies of the electric field effect in the Es layers using simulations in these latitudes.
82   The ionospheric zonal electric field suffers significant modifications in equatorial and low-
83 latitude regions under disturbed conditions. These modifications/disturbances can be classified in
84 two distinct categories: the prompt penetration electric fields (PPEFs), and the disturbance
85 dynamo electric fields (DDEFs) [*Balan et al., 2008; Blanc and Richmond, 1980*]. The
86 interplanetary electric field is related to the IMF B_z component of the interplanetary magnetic
87 field and to the solar wind velocity (V_{SW}). During a southward incursion of IMF Bz, we have an
88 undershielding electric field which penetrates into the ionosphere with eastward (westward)
89 polarity in the day (night) side of the Earth. A reversal of the IMF Bz to north generates an
90 overshielding condition in which the electric field is westward (eastward) during day (night),
91 being in opposite direction do the undisturbed dynamo electric field [*Nogueira et al., 2011*]. The
92 DDEFs, on the other hand, occur due to energy input into the high latitude ionosphere that results
93 into Joule heating and collisional interactions that drive disturbance thermospheric winds toward
94 the equator, creating a disturbed dynamo electric field. They generally occur a few hours after
95 the energy input at high latitudes, generally during the later phases of the geomagnetic storms
96 and have opposite direction to the quiet time electric fields [*Santos et al., 2016*]. In both cases,
97 the disturbed electric fields alter the F region plasma in the ionosphere and can cause some
98 modification in the Es layers as well [*Abdu et al., 2009b*].
99   This paper analyzes the strong Es layer observed in the ionograms at a low latitude region,
100 Boa Vista (BV, 2.8°N, 60.7°W, dip = 18°) in January 2016. We evaluate the significantly
101 enhanced Es layer during the recovery phase of a magnetic storm, in which we attributed such
102 enhancement to the DDEF influence. We used an Es layer numerical model, named MIRE, with
103 a novel neutral wind input to analyze the electric field influence in the Es layer formation over
104 the BV region. Finally, we present a deep study of the possible causes of such strong Es layers
105 that are occurring in BV using simulations and measurements obtained from the ionosondes.

2 Ionospheric Data and Modeling

107   Data from digisonde (DPS-4D) are collected and analyzed in order to get information on
108 F-layer and Es parameters at BV and other stations: Campo Grande (CG, 20.5°S, 55°W, dip = -
109 17°), São Luís (SLZ, 2.5°S, 44.3°W, dip = -3.8°), and Fortaleza (FLZ, 4°S, 38°W, dip = -9°). We
110 have also analyzed the Total Electron Content (TEC) data obtained from a network of Global
111 Navigation Satellite System (GNSS) receivers in South America to verify the response of
112 equatorial and low latitude ionosphere during a magnetic storm. Additionally, the Global Scale
113 Wave Model (GSWM-00) is used as input to MIRE for the selected Brazilian regions. The

114 interaction of the electric fields with the Es layer dynamics was studied for the intense
115 geomagnetic storm of January 2016. In the following, we briefly describe each set of data and
116 models used in this work.

117 **2.1 Digisonde Data**

118 Digisonde is a radar that operates at frequencies ranging from 1 to 30 MHz. It generally
119 operates continuously, making a complete sweeping every 10/15 min [*Reinisch et al., 2009*]. The
120 data provides the ionospheric profile in graphs of frequency versus virtual height, from which it
121 is possible to get the ionospheric parameters for the F and E regions with Es layers. In this study
122 we used the following parameters: the Es blanketing frequency (*fb*Es), which corresponds to the
123 frequency up to which the Es layer blocks the transmitted electromagnetic wave; and the top
124 frequency (*ft*Es), which is the maximum frequency that was reflected from the Es layer.
125 Furthermore, to study the magnetic storm effect in the ionosphere as a whole, we also analyzed
126 the F regions parameters, as the height of the F- layer peak density (*hm*F2) and the vertical drift
127 velocity (V_z).

128 The V_z is obtained by the relation $\Delta hF / \Delta t$, in which the *hF* is calculated using true
129 heights at specific plasma frequencies 4, 5, and 6 MHz. In fact, we used the mean of the drift
130 values calculated at the three frequencies, which was used to represent the height averaged
131 vertical drift of the bottom side F region. More details about this methodology can be found in
132 *Abdu et al. [2010]*.

133 It is important to emphasize that all the ionospheric parameters derived from digisonde
134 data were manually checked since significant discrepancies can be found between the
135 automatically scaled and the true values at Brazilian region. Additionally, further information on
136 the ionosonde model, data availability, and other parameters related to these ionospheric
137 observatories can be found in the review by *Denardini et al. [2016]*.

138

139 **2.2 GNSS TEC Variation**

140

141 The frequency radio signals from the GNSS receiver measures the total number of
142 electrons (TEC) in a column of unit cross-section area between the satellite and the receiver. The
143 TEC values are made available at the website of the Brazilian Studies and Monitoring of Space
144 Weather (Embrace - http://www2.inpe.br/climaespacial/portal/en/), which produces the
145 ionospheric maps. Specifically, we have obtained two-dimensional maps of the absolute vertical
146 TEC values at 10 min time resolution and 0.5°×0.5° of spatial resolution in latitude and longitude
147 in this analysis. The methodology was developed by *Otsuka et al. [2002]*, and the description for
148 the Brazilian sector can be found in *Takahashi et al. [2016]*.

149

150

151 **2.3 MIRE Model**

152

153 We simulated the Es layers using a theoretical model, called MIRE (the Portuguese
154 acronym for E-Region Ionospheric Model), which provides the E region electron density. This is
155 accomplished by solving a system of differential equations of the continuity and momentum for
156 the molecular/atomic (NO^+, O_2^+, N_2^+, O^+) and metallic (Fe^+, Mg^+) ions. The system was solved

157 using 0.05 km grid spacing in height, and 2 min time step between 00 LT and 24 LT. In this
158 analysis, we used the height range from 86 to 120 km. Notice that MIRE can be used for heights
159 up to 140 km, but the GSWM-00, which is used to calculate the input winds for MIRE, does not
160 provide data above 120 km, which is the source of the altitude limitation of this study. More
161 details about the equations and implementation of MIRE can be seen in *Carrasco et al. [2007]*
162 and *Resende et al. [2017a]*.
163 The Es layers formation dynamics can be analyzed by the vertical velocity of the ions:
164
165

$$V_{iz} = \frac{\omega_i^2}{(v_{in}^2 + \omega_i^2)} \left[\cos I \cdot \sin I \cdot U_X + \frac{v_{in}}{\omega_i} \cdot \cos I \cdot U_y + \frac{1}{v_{in}} \frac{e}{m_i} \cdot \cos I \cdot \sin I \right. \tag{5}$$
$$\left. \cdot E_x + \frac{e}{\omega_i m_i} \cdot \cos I \cdot E_y + \frac{e}{v_{in} m_i} \cdot \left(\frac{v_{in}^2}{\omega_i^2} + \sin^2 I \right) \cdot E_z \right]$$

166
167 where ω_i is the ion gyrofrequency, v_{in} is the ion-neutral collision frequency, I is the magnetic
168 inclination angle, m_i is the mass of the ion, e is the electric charge of the ion, E_x, E_y, and E_z, are
169 the electric field components, and U_x is the meridional and U_y is the zonal wind components in
170 the E region. Here, the X-axis points towards the south, the Y-axis points towards the east,
171 whereas the Z-axis completes the right-handed coordinate system, pointing up.
172 In the previous works that used MIRE, the wind model was obtained by the fitting of amplitude,
173 wavelength, and phase parameters computed from the observational data of the meteor radar
174 installed in Brazilian low-latitude regions [*Resende et al., 2016; Resende et al., 2017a; Resende*
175 *et al., 2017b; Moro et al., 2017*]. However, there is no meteor radar available near BV. Thus, in
176 the present study, it was necessary to use a theoretical model, the GSWM-00, which successfully
177 described the wind dynamics over the regions near geographic equator [*Hagan et al., 2002,*
178 *2003, Buriti et al., 2008*]. Details about the GSWM-00 can be seen on the website of the High
179 Altitude Observatory (HAO) of the National Center for Atmospheric Research (NCAR), in
180 Colorado (http://web.hao.ucar.edu/public/research/tiso/gswm/gswm.html).
181 Using GSWM-00, we obtain the semidiurnal (12h) and diurnal (24h) amplitudes, the
182 phase, and the wavelength for zonal and meridional tidal wind components in BV. Then, the tidal
183 components can be computed by:
184

$$U_x(z) = U_{x0}(z) \cdot \cos\left(\frac{2\pi}{\lambda_x}(z - z_0) + \frac{2\pi}{T}(t - t_{x0}(z)) \right) \tag{5}$$

185

$$U_y(z) = -U_{y0}(z) \cdot sin\left(\frac{2\pi}{\lambda_y}(z - z_0) + \frac{2\pi}{T}\left(t - t_{y0}(z)\right)\right), \tag{6}$$

where $U_{x0}(z)$ e $U_{y0}(z)$ correspond to wind amplitudes at the height z; λ_x and λ_y denote the wavelengths; T is the period of the tide (24h for diurnal and 12h for semidiurnal); z_0 is a reference height assumed as 100 km; and $t_{x0}(z)$ and $t_{y0}(z)$ are the wave phases.

Figure 1 shows the temporal and altitudinal variation of the meridional (Figure 1a) and zonal (Figure 1b) wind profiles of the tidal modes that were included in MIRE to simulate the Es layers over BV. It is important to mention here that the GSWM-00 was used as input in MIRE model for the first time, which required validation before carrying out the analysis of the electric field effects.

The null points (zero curves) indicate the wind shear mechanism that is necessary to form the Es layer. The zonal amplitude is larger (max ~ 25 m/s) than the meridional amplitude (max ~ 17 m/s), in agreement with the observational results obtained previously for other Brazilian regions [*Resende et al., 2017a; Resende et al., 2017b*]. However, the wind amplitudes are lower in BV than at other Brazilian regions analyzed before. Hence, it is expected the Es layers to be very weak in BV in most days, which agrees with the numerical results obtained from MIRE as will be shown in Section 3.
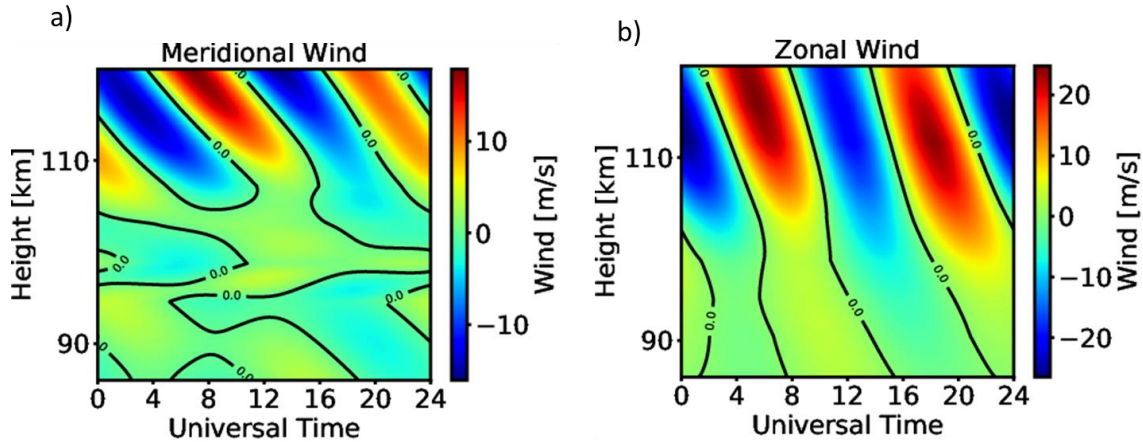
Figure 1. Wind profile of the meridional (a) and zonal (b) obtained by GSWM that was included in MIRE to simulate the Es layers over BV.

3 Results and Discussion

3.1 Magnetic storm Event

Figure 2 shows the variations of the interplanetary magnetic field (IMF) B_z component (a), the solar wind speed (V_{SW}, km/s) (b), the Dst index (nT) (c), and AE, auroral electrojet (nT) index (d) for the 18-25 January 2016 geomagnetic storm. The B_z and V_{SW} parameters were taken from the OMNIWeb database, which were obtained from the Advanced Composition Explorer

214 (ACE) satellite measurements. The AE and Dst indices were obtained from the World Data
215 Center from Geomagnetism, Kyoto.
216   The coronal mass ejection (CME) arrived in the Earth's magnetosphere on 19 January
217 2016 at 1000 UT, causing an abrupt increase in the B_z component. The CME effect lasted until
218 January 21, 2016, when the Earth's environment starts to recover. Additionally, the Bz
219 component turned southward (negative) from about 0530 UT on 20 January to 0400 UT on 21
220 January. The Dst index started to decrease (magnetic storm main phase) at around 0100 UT on
221 20 January, reaching almost -100 nT at 1600 UT, which is the threshold for classifying it as an
222 intense storm according to the classification by *Gonzalez et al. [1994]*. Afterward, it is possible
223 to observe a slow recovery of the Dst index that lasted until 23 January. The V_{SW} increased
224 gradually from about 320 km/s to almost 600 km/s. Furthermore, the AE index showed a peak of
225 ~1250 nT around 1500 UT on 20 January. After this peak, the AE had an oscillating behavior
226 with values between 200 nT and 500 nT.
227
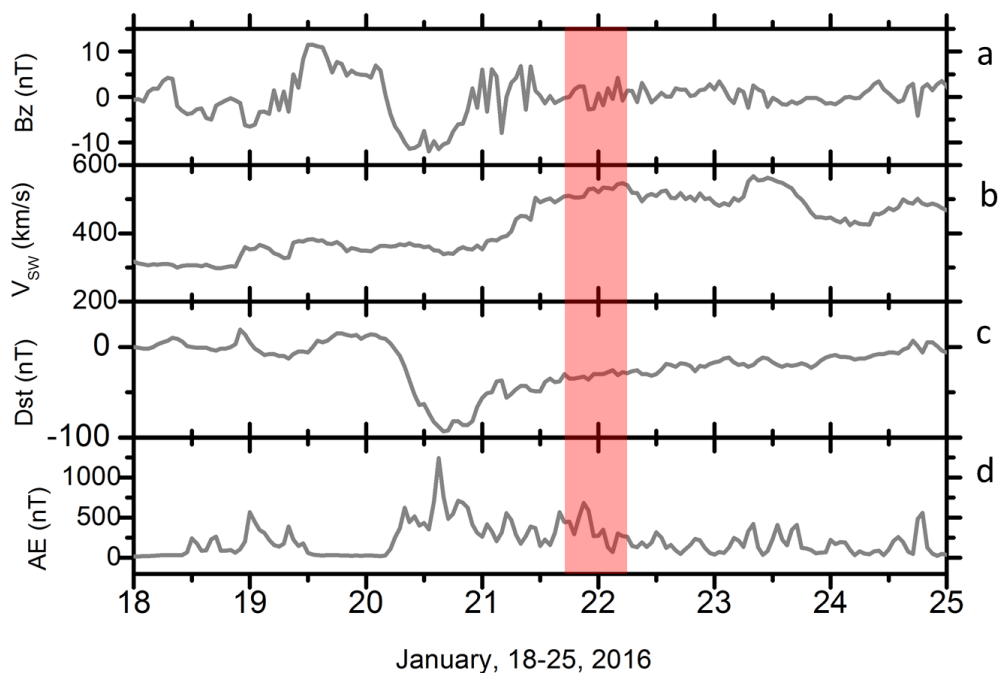
Figure 2. IMF Bz, solar wind speed, Dst, and AE auroral electrojet indices (UT) from 18 to 25 November 2016.

3.2 Strong Es layer in BV

233   During part of the magnetic storm recovery phase that occurred on 21-22 January 2016,
234 we observed strong Es layers in BV, which is not the typical behavior at that location. This layer
235 occurrence starts at 2330 UT on 21 January and it lasts until 0640 UT on 22 January, when it
236 starts to weaken. Therefore, although we are showing the data obtained from the days around the
237 magnetic storm that occurred on 20 January, we will focus only on the shaded area of Figure 2.

238   Figure 3 shows the Es layers in ionograms (red arrow) between 2330 UT on 21th and
239   0700 UT on 22th January 2016, in increments of half an hour. During this time, the *ft*Es
240   oscillated between high and low values. In fact, between 2330 UT and 0100 UT, the *ft*Es reached
241   values even higher than 15 MHz (at 0050 UT, not shown here). After, the Es layer started to
242   weaken, but it strengthened again in the next hours (see 0300 UT). This oscillation lasted until
243   0700 UT, when the Es layer began to disappear. In the hours following 0700 UT, the Es layers
244   returned to its typical behavior with a not significant density (not shown here).
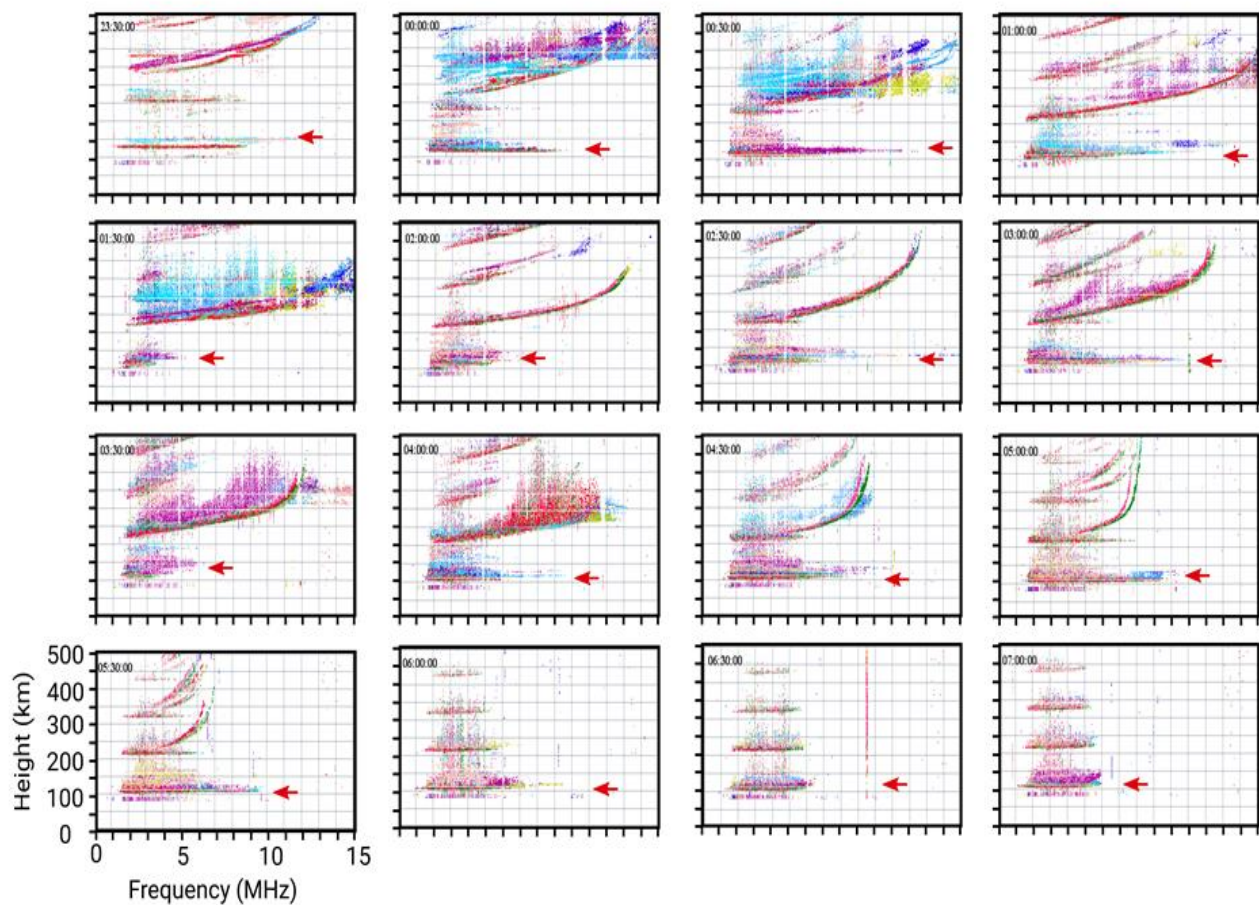
245
246
247   **Figure 3.** Ionograms at Boa Vista collected from 2330 UT on 21th January 2016 until 0700 UT on 22th January
248   2016, showing the atypical strong Es layers.
249

250   Similar strong Es layers were observed in BV ionograms during the recovery phase of all
251   the magnetic storms shown in Table 1. We have selected the moderate/intense magnetic storms
252   (Dst < -50) that occurred in 2016 and 2017, a period in which we had data available for the BV
253   region. Notice that all density increases occurred during the magnetic storm recovery phase. As it
254   will be discussed later, these layers cannot be formed by wind shear mechanism only, since the

255 tidal winds in the regions near the geographic equator, as BV, have small amplitudes in their
256 meridional and zonal component (Figure 1). Therefore, another mechanism must be acting at this
257 region to form these strong layers.
258
259
260 Table 1: List of strong Es layer in BV associated to moderate/intense magnetic storms (Dst < -50) in 2016 and
261 2017.

Arrival of the CME on Earth	Minimum Dst (nT)	Beginning of the strong Es layer observation	Magnetic Storm Phase of Es layer observation
05 March 2016; 1900UT	-98	06 March 2016; 2140 UT	Recovery
13 October 2016; 0600UT	-104	14 October 2016; 2350UT	Recovery
04 November 2016; 1800UT	-50	04 November 2016; 2350 UT	Recovery
10 November 2016; 0000UT	-59	12 November 2016; 2000 UT	Recovery
27 May 2017; 2200UT	-125	30 May 2017; 2050 UT	Recovery
16 July 2017 1500UT	-72	17 July 2017 2310 UT	Recovery

262
263   In face of such observation at BV, we looked for strong Es layers in the same data
264 collected in other regions aiming to define the geographical/geomagnetical extent of such
265 phenomena. Figure 4 shows the *fb*Es (green line) and *ft*Es (orange line) parameters between 21
266 and 23 January 2016 for four different low latitude regions in Brazil, BV, CG, FLZ, and SLZ.
267 The FLZ and SLZ are regions close to the magnetic equator, whereas CG is located at the same
268 magnetic meridian as BV, but in the Southern Hemisphere. From this figure, it is clear that the
269 high top frequency values of the Es layer, i.e. the higher electron density, were only observed in
270 BV. For the FLZ and SLZ regions, the *ft*Es/*fb*Es during the nighttime had low values, and it
271 disappeared in few hours.
272   Once we have no wind measurements in these regions (SLZ and FLZ), associated with
273 the GSWM-00 output showing not enough wind shears to form Es layers, the Es layer modeling
274 at the Brazilian regions faces some difficulties. Nevertheless, we recall that *Resende et al.*
275 *[2017b]* studied the wind behavior to form Es layers using an all-sky interferometric meteor
276 radar installed in São João do Cariri (7.23S, 36.32W, dip: -22.16), the nearest region to São Luís.
277 They observed that the Es layer electron density in São Luís has low values during the day,
278 disappearing in the night hours. This behavior agrees with the observations on SLZ and FLZ in
279 the analyzed period here. The authors concluded that the zonal wind component was found to be
280 the most important for the Es layer formation, and this component at a nearby equator station has
281 low amplitudes forming weak Es layers. Furthermore, in some hours for these regions, the *fb*Es
282 shows a typical behavior characterized by an enhancement during the morning period, starting
283 about 09 UT (06 LT), and reaching maxima values about 15 UT (12 LT), followed by a steady
284 decrease, reaching the quiescent values after 21 UT (18 LT) [*Resende et al., 2017a*]. For all these
285 reasons, the Es layers in SLZ and FLZ do not have any atypical behavior as in BV.
286   Regarding CG (panel b), the Es layer completely disappeared at the moment of the
287 occurrence of the strong Es layers in BV. In fact, the CG is located at the same magnetic
288 meridian as BV, meaning that the integrated field line conductivity is the same in both these
289 regions [*Abdu et al., 2009a*]. *Batista et al. [2008]* studied the relation between the spread F (SF)
290 occurrence and Es layer characteristics using simultaneous data to look for any possible relation
291 between these two phenomena in BV, CG, and Cachimbo (9.8S, 54.5W). Several instruments

292 were provisionally installed in these stations during the Conjugate Point Equatorial Experiment
293 (COPEX) campaign, which occurred in Brazil from October to December 2002. They did not
294 detect any significant correlation between the SF occurrence/generation at the magnetic equator
295 and the presence of Es layers at the conjugate E regions along the same field line. However, they
296 observed that the Es layers were stronger in BV when compared to those detected in CG.
297 Nevertheless, they did not study the effect of the vertical equatorial electric field (that is
298 associated with the eastward electric field pre-reversal enhancement) with the Es development or
299 disruption.
300   Lastly, the digisonde installed recently in BV allows the analysis of the recurrent atypical
301 Es layer during the recovery phase of the magnetic storm. In this context, we performed a deeper
302 analysis of the magnetic storm period in January 2016 to find a possible explanation of such
303 behavior in BV.
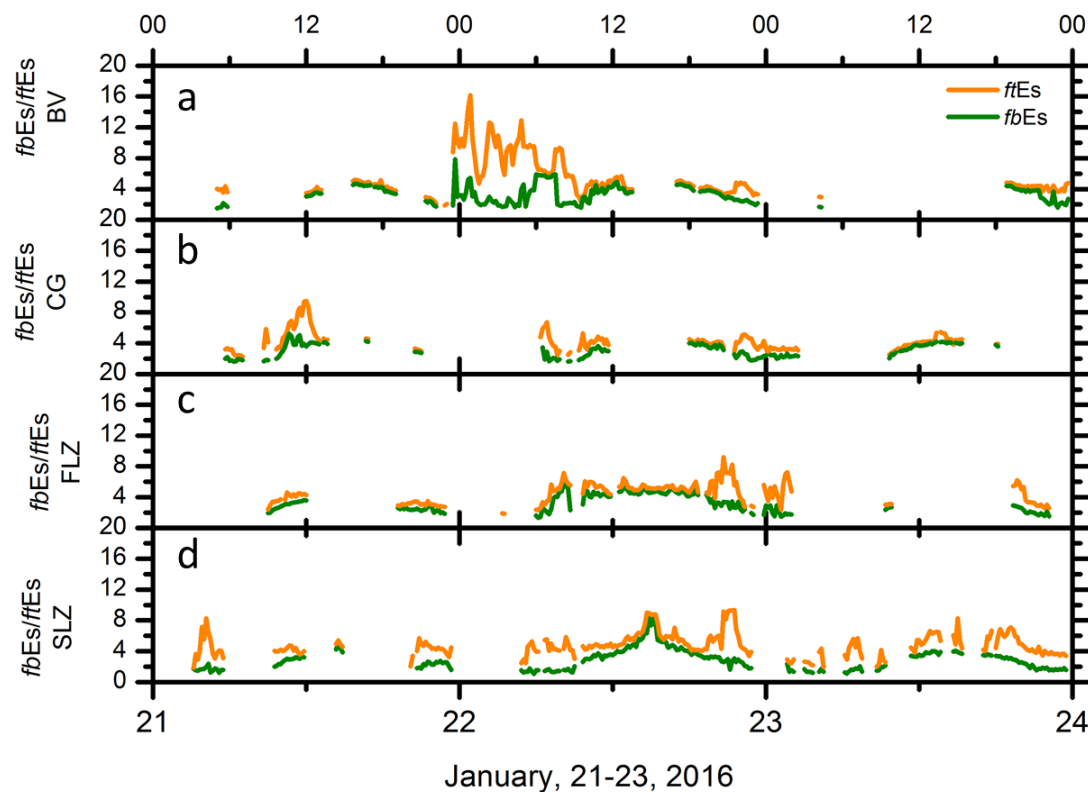
304
305 **Figure 4.** The *fb*Es and *ft*Es parameters at four Brazilian: low latitudes, Boa Vista (panel a), Campo Grande (panel
306   b), and equatorial regions, Fortaleza (panel c), São Luís (panel d) on 21-23 January 2016.
307

3.3 The F region effect

309
310   Figure 5a presents the F2 layer peak height (*hm*F2) parameter for 21 and 22 January 2016
311 over BV. The blue line refers to a quiet day (January 18) used as reference. An important
312 characteristic observed in this Figure is that the F layer peak height enhancement near sunset
313 (hachured area) was reduced in relation to the quiet period. The possible causes for this *hm*F2

314   reduction can be either 1) a northward meridional wind which contributes to the lowering of the
315   layer, 2) a reduction of the eastward electric field through an overshielding effect of a PPEF or 3)
316   a westward disturbance dynamo electric field (DDEF). In the present case it seems that the
317   meridional wind is directed southward as we can see in Figure 5b. This Figure presents the
318   difference between *hm*F2 measured at CG and BV (d*hm*F2 = *hm*F2$_{CG}$ − *hm*F2$_{BV}$), which, as
319   discussed in *Abdu et al. [2009a]* and in *Batista et al. [2017]*, is a measure of the
320   interhemispheric symmetry/asymmetry in *hm*F2. Positive/negative values of d*hm*F2 indicate
321   transequatorial meridional wind (TMW) directed northward/southward. As it can be seen from
322   Figure 5b, at the time of the *hm*F2 reduction over BV, d*hm*F2 is negative, indicating a southward
323   TMW. Such a TMW would contribute to increase the F layer height over BV which is not
324   observed in the data. The second hypothesis of an overshielding PPEF would occur under the
325   presence of northward turning of the IMF-B$_z$, which was not observed during the time interval
326   under consideration. In fact, B$_z$ is close to zero and AE presents minor fluctuations (see Figure
327   2). Therefore, it seems that a westward disturbance dynamo electric fields (DDEF) is the most
328   probable candidate to explain the reduction in the rise of F layer peak height during the time of
329   interest for this study.
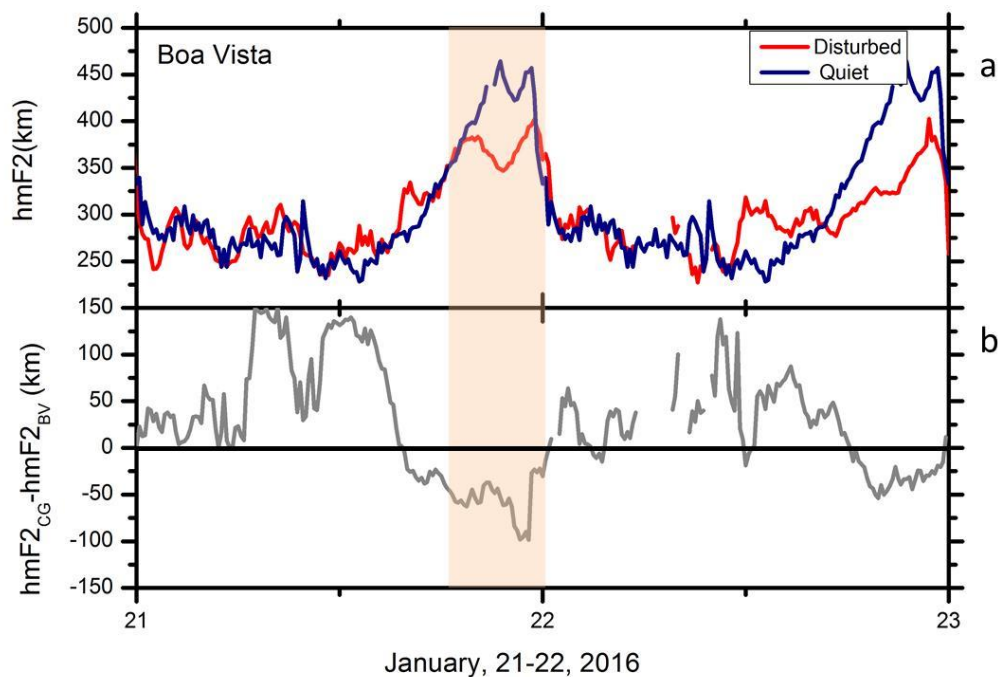
330
331   **Figure 5.** The *hm*F2 parameter at Boa Vista (panel a) and the difference between hmF2 in Campo Grande and Boa
332   Vista (panel b) on 21-23 January 2016.
333

334   To confirm the DDEF effect in the F-layer height, we calculated the ExB drift during the
335   hours when the strong Es layers were observed. In order to perform this calculation, it is
336   important to have in mind that the vertical drift velocity using the relation mentioned before
337   (Δ*hF*/Δt) is valid near sunset and night hours when the F-layer height is equal or higher than 300

338 km. If the layer is below this height, then the recombination processes need to be taken into
339 account for the drift velocity calculation. Thus, the vertical drift velocity is given by
340

$$V_{BV} = V_{ap} - \beta H, \tag{1}$$

341
342 where the V_{BV} refers to the drift velocity at Boa Vista (BV), V_{ap} is the apparent vertical drift
343 (measured) for a station, β is the recombination coefficient, and H is the scale height of
344 ionization. The recombination coefficient is given by
345

$$\beta = k_1[N_2] + k_2[O_2]. \tag{2}$$

346
347   The reaction coefficients k_1 and k_2 can be found in *Nogueira et al. [2011]*, and $[N_2]$ and
348 $[O_2]$ are the neutral molecular nitrogen and oxygen number densities, respectively, which were
349 obtained from the atmospheric model MSISE-90 *[Hedin et al., 1991]*.
350   Additionally, for stations located outside the magnetic equator, like BV, we need to
351 consider the meridional wind since this component may contribute to the vertical plasma motion
352 as well [*Rishbeth et al., 1978; Nogueira et al., 2011*]. Therefore, V_{ap} is given by:
353

$$V_{ap} = V_D \cos I \pm U_F \cos I \operatorname{sen} I - w_D \sin^2 I, \tag{3}$$

354 where V_D is the vertical drift velocity calculated as $\Delta h / \Delta t$, I is the magnetic inclination angle (
355 ~18° in BV), U_F is the meridional wind in the F region (positive northward), w_D is the
356 contribution to the vertical plasma velocity due to diffusion given by $w_D = g/v_i$, where g is the
357 acceleration of gravity, and the v_i is the ion-neutral collision frequency. We used the same
358 methodology described in *Nogueira et al. [2011]*, in which v_i is computed as:
359

$$v_i = 4.34 \times 10^{-16} [N_2] + 4.28 \times 10^{-16} [O_2] + 2.44 \times 10^{-16} [O], \tag{4}$$

360
361 where $[N_2]$, $[O_2]$, and $[O]$ were obtained from MSISE-90.
362
363   The vertical drift calculated according to the above equation is shown in Figure 6. The
364 grey line in the Figure refers to the quiet period drift whereas the orange line refers to the
365 recovery phase of the magnetic storm that we call disturbed period. Positive/negative drift values
366 are directed to the east/west. Notice that the DDEF effect can be clearly seen, since, during the
367 PRE hours (2100 UT), the ExB drift was inhibited, presenting opposite direction of the typical
368 quiet time behavior. After these hours, the drift velocity tried to recovery and reached values
369 higher than the quiet drift velocity. Finally, after 0200 UT, the drift velocity presented an
370 oscillatory behavior, showing that the drift was returning to its typical values.
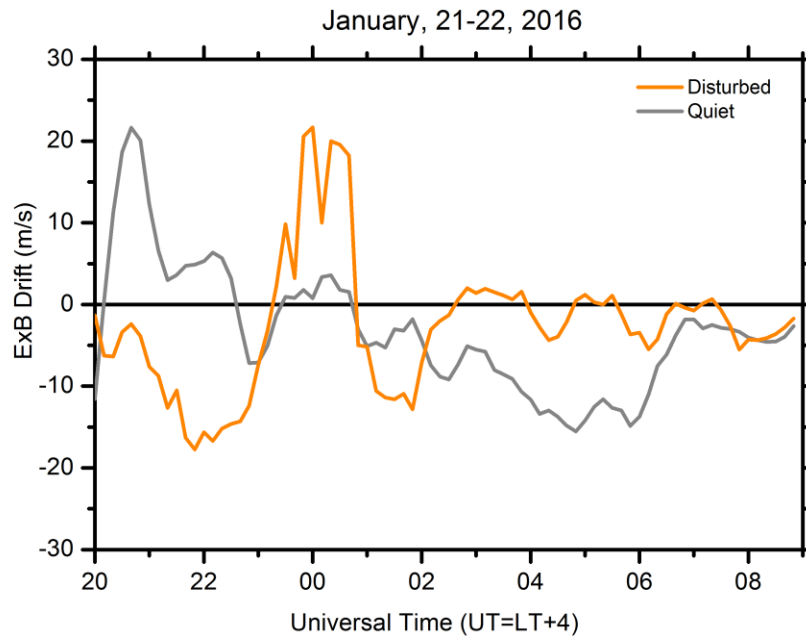
Figure 6. The ExB drift in quiet (grey line) and disturbed (orange line) periods between the 2000 UT and 0900 UT at Boa Vista on 21-22 January 2016.

Generally, the DDEF show low values of downward disturbance drifts between 0700 and 1700 LT, followed by larger downward drifts near sunset and upward drift near midnight. The local time and seasonal dependence of the disturbance dynamo drifts are largely anti-correlated with those of the prompt penetration drifts or quiet time drift [*Fejer et al., 2008*], which seems to be in agreement with the results presented in Figure 6. We also analyzed the equatorial ionization anomaly (EIA) modification using TEC Maps over South America to observe and confirm the presence of the DDEF effect. Figure 7 shows the TEC over South America. The solid black line across the map indicates the magnetic equator location in 2016. In Figure 7a we have the TEC Map during the reference quiet day (18 January 2016). Notice that the EIA crests are well demarked at low latitude stations (yellow colors in maps) between 2100 UT and 2300 UT, which is the typical behavior of the ionosphere plasma over Brazil. On 21 January 2016, it is possible to observe a clear weakening of the EIA crest near sunset time (Figure 7b). Similar behavior was observed in a study by *Nogueira et al. [2011]*, in which they analyzed the response of the ionosphere during two magnetic storms that occurred in 2001. In fact, they analyzed the EIA intensity and the variations in the zonal electric field in different phases of the magnetic storms. They found that the PPEF mechanism occurred during the main phase in both cases, causing an enhancement in the EIA. However, during the recovery phase, they found that the DDEF almost caused an EIA crest disappearance, agreeing with our results.

We emphasize here that this mechanism is a global phenomenon. Thus, the westward electric field in PRE hours due to disturbance dynamo occurs in all regions of Brazil, being more visible in those near the magnetic equator.
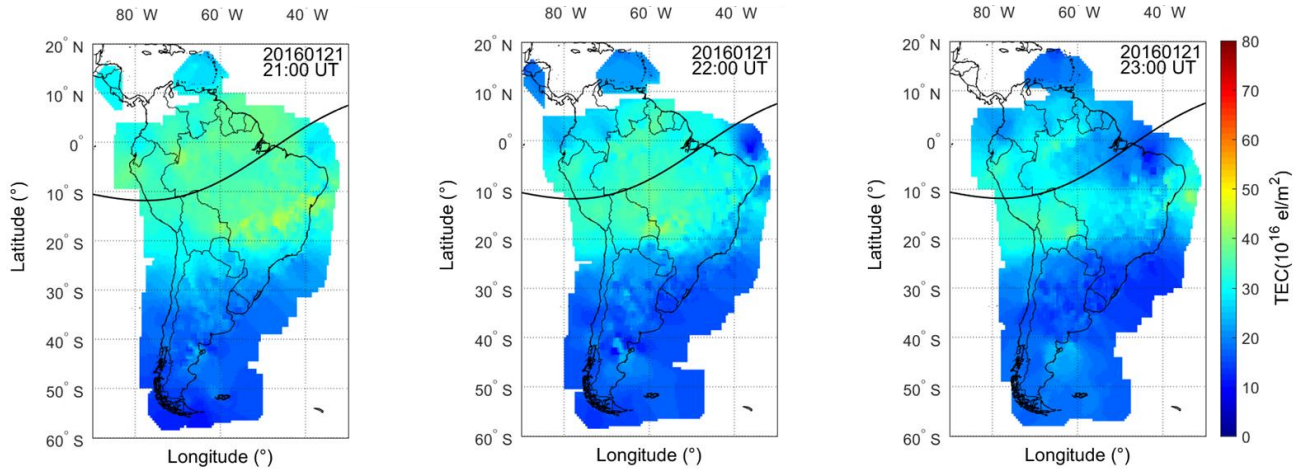
January, 18, 2016

a)

January, 21, 2016

b)
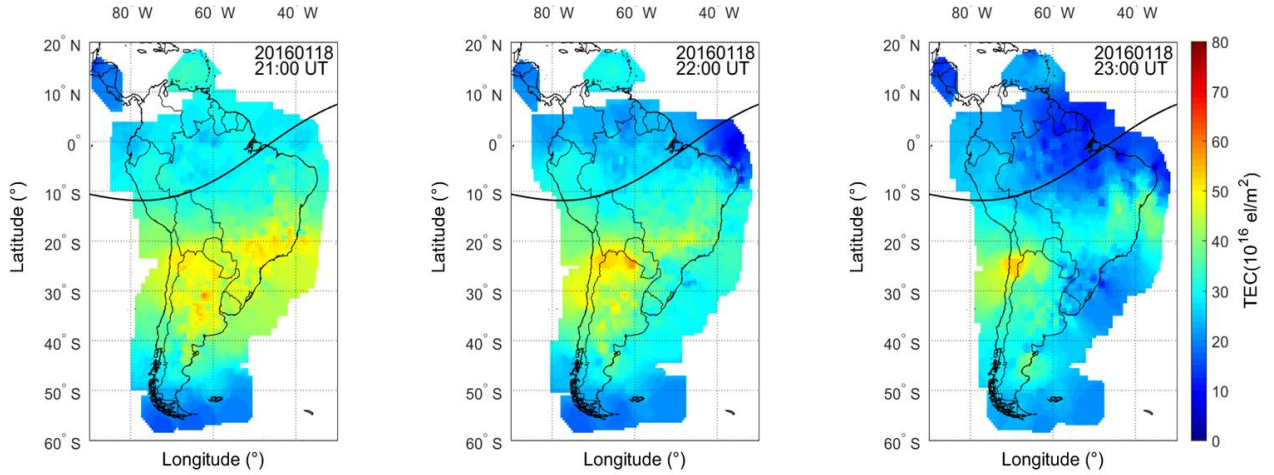
398
399
400   **Figure 7.** Longitude versus latitude distribution of the TEC Map over South America at one hour interval
401   during (a) the quiet time period, and (b) covering the period of the disturbance dynamo effect.
402
403   Therefore, the inhibition of the PRE drift and EIA are concrete evidences of the influence
404   of a DDEF that occurred in the recovery phase of the 20 January magnetic storm, as already
405   discussed by several authors [*Sastri et al., 1988; Abdu et al, 1997; Abdu et al., 2006; Santos et
406   al., 2012*]. Thus, we believed that the strong Es layer formation on BV can be influenced by the
407   DDEF. This fact was analyzed in detail and it is shown hereafter.

408
409 **3.3. Analysis of the electric field effect using simulations**
410
411   In this work we are pointing out that the only possible mechanism to form the strong Es
412 layers in BV is due to an electric field superposed to the wind shear mechanism. According to
413 *Fejer and Scherliess [1995]* the relationship between the zonal electric field and the vertical drift
414 produced by this electric field is approximately 1 mV/m to 40 m/s. Analyzing Figure 6, the drift
415 during the hours of the PRE was approximately -20 m/s, which corresponds to a westward
416 electric field of 0.5 mV/m. Comparing with the ionograms in Figure 2, the strong Es layer starts
417 to occur at 2330 UT, shortly after the electric field reached its highest value. After, the Es layer
418 tries to return to normal conditions, around 0130 UT, when the *fb*Es and *ft*Es reached the lowest
419 values in this period. At the same time, the drift velocity on January 22, 2016 showed a positive
420 value of ~15 m/s, meaning an eastward electric field of approximately 0.42 mV/m. However, at
421 0200 UT, the drift velocity became negative, meaning that the zonal electric field is westward
422 again. At 0230 UT, the *ft*Es reached values higher than 15 MHz, but this behavior did not last
423 long since the vertical drift oscillated in the next hours. Thus, this result shows a possible
424 connection between the westward electric field and the Es layers formation.
425   We included the electric field values in MIRE to verify this behavior. First, we included a
426 constant westward electric field equal to 0.5 mV/m between 2000 UT and 0600 UT that
427 corresponds to the PRE vertical drift of -20 m/s. Figure 8 show Height-Time (HT) Maps of the
428 electron density profile simulated by MIRE (color scale) over BV on January 22, 2016. The
429 background color maps show a typical behavior of the E region electron density, with low values
430 in the night period and expressive electron density in the daytime. In Figure 8a, we considered
431 only the wind effect obtained by the GSWM-00. Notice that MIRE successfully simulated the Es
432 layers, which are observed as the thin descending layers in some hours. The Es layers were
433 formed around 110 km with low density and a downward movement is observed, agreeing with
434 the theory about the Es layer behavior [*Bishop and Earcle, 2003; Haldoupis et al., 2006*]. This
435 scenario is typical for Es layers formed by the wind shear mechanism [*Resende et al., 2017b*].
436 Furthermore, notice that the Es layer did not seem to occur during the daytime since its density
437 was very close to the background E region density. However, in the nighttime, which is our
438 interest in this study, the Es layers were clearly observed.
439   Figure 8b shows the HT Maps of electron density profile simulated by MIRE with the
440 selected constant value for the electric field. It is possible to observe that the Es layer during the
441 night hours were stronger when it was compared with Figure 8a. From 18 UT, the density layer
442 increased significantly, approximately 1.5 times more. During the first hours of the morning
443 (0000 UT until 0400 UT), the Es layer density when considering the electric field reached almost
444 10^5 electrons/cm^3, whereas the Es layer formed only by the winds reached a density of
445 approximately 10^4 electrons/cm^3. Therefore, the constant westward electric field caused a
446 strengthen to these Es layers in BV.
447
448
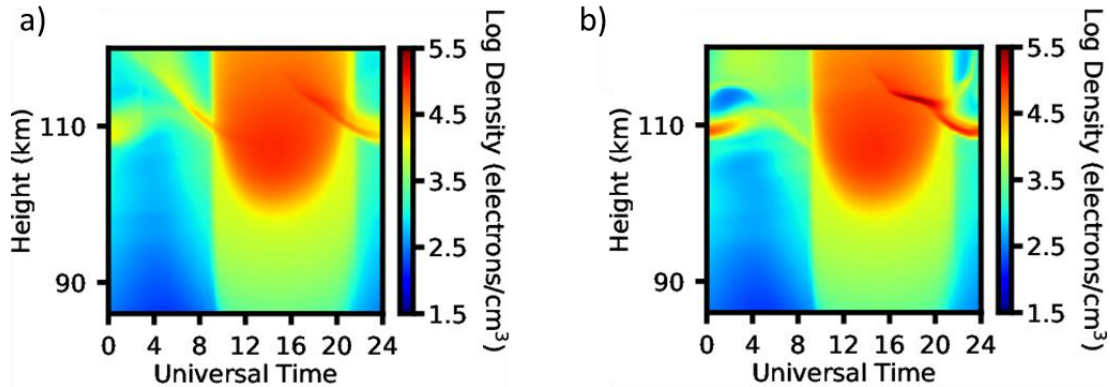
Figure 8. Electron density as a function of Universal Time (UT) and height (km) simulated by MIRE considering the diurnal and semidiurnal tidal winds representative of January 2016 (a) and considering the westward zonal electric field component of 0.5 mV/m (b).

It is possible to notice in Figure 8b that the constant electric field included during the nighttime in MIRE caused modifications to the Es layer profile. *Resende et al. [2016]* and *Moro et al. [2017]* showed that the zonal electric field can cause a modulation in the existing Es layers, which is still attributed to the tidal wind mechanism. They studied the equatorial regions electric field due to the EEJ current to analyze the Es layer formation, concluding that the zonal electric fields are not efficient enough to create or disrupt any Es layers. The only observable effect is some modulation. Therefore, in our case, it was possible to confirm that the electric field caused some influence in diurnal times.

Carrasco et al. [2007] analyzed the vertical electric field influence in the Es layers during the F region pre-reversal enhancement (PRE) in the zonal electric fields by mapping these electric fields through the equipotential magnetic field lines. Depending on the direction of the vertical electric field component, they observed an Es layer disruption or enhancement around the sunset and its correlation with the PRE. In fact, a vertical electric field during the sunset can be mapped to low latitudes regions, causing some influence in the Es layers. On the other hand, *Abdu et al. [2014]* investigated the same situation of low-latitude Es layers during the magnetic storm periods. They show that a PPEF of an overshielding electric field with the westward polarity in the evening sector can cause the sporadic E layers formation near 100 km. The deeper analysis performed by them concluded that the ionization of the Es layer formation is driven by the enhanced ratio of field line integrated Hall to Pedersen conductivity $(\sum H)/(\sum P)$ during the magnetic storms, influencing the electric field components in F region. After, the vertical electric field is mapped to E region, which can form strong Es layers. To confirm the enhancement in the $\sum H/\sum P$ ratio, they used the energetic particle precipitation since the regions analyzed are located in the South Atlantic Magnetic Anomaly (SAMA). Therefore, they concluded that during the disturbed periods the electric field effects on Es layers occur more in the SAMA region.

In our study, it was not possible to analyze the influence of the F region vertical electric field mapped to BV, since we do not have measurements in equatorial regions for the same magnetic field line. In fact, this is a possible mechanism due to the absence of the Es layers in CG. The vertical electric field can be mapped to BV and CG, in opposite directions, causing a strengthening and disruption of Es layers, respectively. However, the explanation in *Abdu et al.*

484   *[2014]* about the enhancement in the $\sum H/\sum P$ ratio in SAMA regions is not possible since BV is
485   located far from the northern border of the anomaly.

486   The literature [*Fürst et al., 2009; Ginet et al., 2007*] shows that the BV region is located
487   on the Northwest boundary of the SAMA, which means that this region may receive few
488   influences of the particle precipitation. *Da Silva et al. [2016]*, presented the preferential particle
489   precipitation region on the SAMA through the distribution of the X-Ray (3.0–31.5 keV energy
490   range) of the upper atmosphere measured by RPS (X-ray spectrometer) device on board of the
491   CORONAS-F satellite, in which it is clearly seen that there is no particle precipitation over BV.
492   Even knowing that there is little chance of the charged particle precipitation in the region of the
493   interest, it is extremely important to investigate the dynamic processes on the outer radiation belt
494   during the specific case study (2200 - 0000 UT on January 22, 2016), as following below.

495   The Van Allen Probes data [*Mauk et al., 2012*] showed that the outer radiation belt flux
496   (high-energy, Figure not shown) for this event is considerable stable (without dropout and/or
497   enhancement). The data also showed the absence of the Chorus (from hundreds of Hz up to
498   about 10 kHz) and Electromagnetic Ion Cyclotron – EMIC (0.3 Hz up to 3 Hz) wave activities, it
499   means the pitch angle scattering mechanism [*Kennel and Petschek, 1966; Thorne et al., 2010*]
500   did not occur, consequently charged particles were not launched in the loss cone, resulting to not
501   occurrence the particle precipitation during all period of this case study. Through this
502   investigation may suggest that the Es layers detected here are generated without the influence of
503   the particle precipitation. Therefore, it is concluded that the $\sum H/\sum P$ enhancement which is
504   directly intensified in the SAMA region during the magnetic storms has little or no influence on
505   the mechanisms able to intensify the Es layers on BV region.

506   Another possibility is the direct effect of the DDEF in BV. In fact, the westward electric
507   field can intensify the Es layers as shown in *Abdu et al. [2014]*. Indeed, the fast variation of the
508   electric field from eastward to westward on the night of 21-21 January 2016 may be causing the
509   oscillations in the frequency parameters observed in Figure 3. We believe that the zonal electric
510   field around 0.5 mV/m-1mV/m may have driven plasma densification as proposed by *Dagar et*
511   *al. [1977]*. In their analysis, the values of the zonal component of the electric field, even with
512   winds influence, could form Es layers when their values were smaller than 2 mV/m. Also, *Dagar*
513   *et al. [1977]* found that the zonal electric field component increases the Es layer electron density,
514   and, even if the electric field ceases, it still takes time for the Es layer to disappear completely.

515   Therefore, we analyzed the evolution of the electric fields obtained by the vertical drift of
516   Figure 6. For each value between 2000 UT and 0000 UT, and from 0000 UT to 0600 UT, we
517   calculated the electric field using the relationship in *Fejer and Scherliess [1995]*. Thus, the
518   electric field that was included in MIRE has the behavior presented in Figure 9a, in which the
519   negative and positive values mean the westward and eastward polarity, respectively. In Figure 9b
520   we show the simulation results, in which it is possible to verify that the Es layer is strong during
521   almost the entire day. In some hours during the daytime, the Es disappear. However, our focus is
522   around the nighttime period. Also, the Es layer seems to be weakened around 0400 UT to 0600
523   UT, but right after it becomes stronger again. This result shows that the inhibition of the PRE
524   due to the action of the disturbance dynamo electric field can influence the enhancement of Es
525   layer in our simulations. We believe that this behavior did not occur in CG because the vertical
526   drift was smaller and the electric field was not enough to strengthen the Es layers. Furthermore,
527   the tidal wind configuration in CG is completely different with respect to BV, which may also

528   have influenced the absence of the Es layers. In fact, the GSWM-00 is not effective in forming
529   Es layers far away from the geographical equator [*Resende et al., 2017a*], precluding a deeper
530   analysis for this region.
531
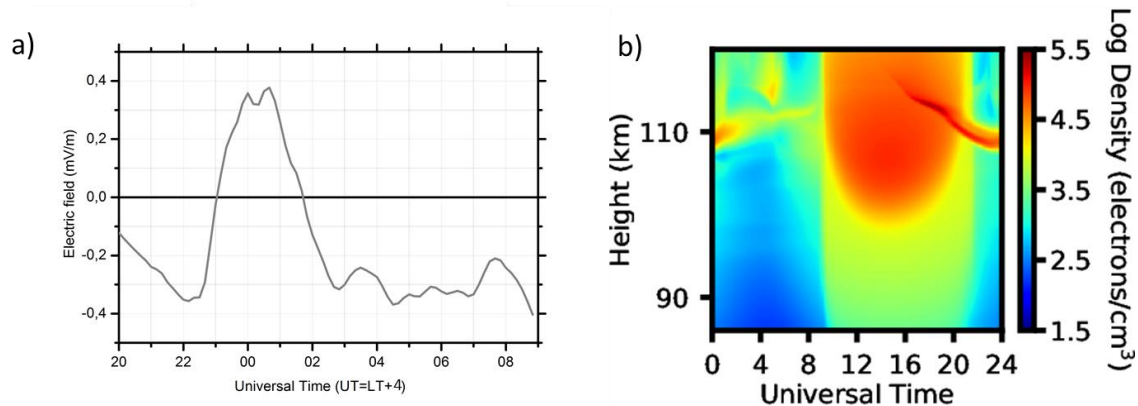
532
533   **Figure 9.** Zonal electric profile between 20 UT and 09 UT on the 21-22 January 2016 (a), and the electron
534   density as a function of Universal Time (UT) and height (km) simulated by MIRE considering the winds and the
535   zonal electric field (b) on BV.
536
537

538   Finally, although there is evidence that the direct DDEF may be influencing the Es layers
539   intensification in BV, the proposal of *Abdu et al. [2014]* cannot be totally discarded. Even BV
540   been outside the SAMA region, the vertical electric fields mapped from equatorial F region to
541   low latitudes can have some influence on the Es layers formation in BV. However, the Es layers
542   in BV appear to be stronger than those observed in the study of *Abdu et al. [2014]*. Besides that,
543   the zonal electric field values used in the previous analysis of the Es layer [*Dagar et al., 1977*]
544   are similar to those of our study, corroborating that the intensifications observed may be
545   associated with DDEF. Furthermore, using simulations for the first time, it was possible to verify
546   that these strong layers in BV are due to the combined effect of these electric fields with the
547   winds. Lastly, it is noteworthy that the influence of the electric fields in the Es layers is a
548   particularity of regions such as Brazil, which has the magnetic equator crossing the country from
549   west to east.

4 Conclusions

551   We have performed in this work a comprehensive analysis of the strong Es layer
552   formation over Boa Vista (BV). These layers are been observed during the recovery phase of the
553   magnetic storms. Therefore, we used the TEC and digisonde data, as well as modeling results to
554   provide some explanation of this behavior.
555   We investigated in detail the ionospheric response to the disturbing electric fields in these
556   atypical Es layers appearance during the magnetic storm of 21-22 January 2016. Our finds reveal
557   that the possible mechanism to form these strong Es layers in BV is due to a disturbed electric
558   field caused by the disturbance dynamo. We performed a deep study around this magnetic storm,
559   and the results show that the Es layer intensification is related to the F-region pre-reversal
560   enhancement inhibition of the vertical drift. This was caused by a westward electric field during

the disturbance dynamo effect. Furthermore, we confirmed the disturbance dynamo occurrence using the TEC Maps over South America, which showed the weakness of the equatorial ionization anomaly crest.

After that, we quantified the electric field influence using MIRE model including the winds obtained by the GSWM-00. In fact, the wind shear mechanism is the main agent to form a weak Es layer in BV. We believe that the disturbed electric field due to the disturbance dynamo was superposed to the wind shear mechanism, forming these strong Es layers. Thus, we used the relationship between the zonal electric field and the vertical drift to obtain the electric field values to simulate Es layers in MIRE. The results show that a constant westward electric field equal to 0.5 mV/m or an evolution of the electric fields obtained by the vertical drift along the day caused a significant Es layer electron density enhancement in simulations. This behavior occurred only when the disturbance dynamo was effective.

Additionally, we analyzed the other possible causes of such strong Es layers that are occurring in BV to confirm that the disturbance dynamo electric field is the main formation agent of these Es layer. We verify that the enhancement in the $\sum H/\sum P$ ratio can be a possible mechanism to form denser Es layers. However, this enhancement occurs in regions near of the South Atlantic Magnetic Anomaly, which can have energetic particle precipitation. Therefore, in Boa Vista this mechanism is not effective since this region is located far from the northern border of the anomaly.

Finally, the combined results from the model and observational data confirmed that these atypical Es layers are due of the disturbance dynamo electric field. Thus, it is noteworthy that the influence of the electric fields in the Es layers is a particularity of regions such as Brazil, which has the magnetic equator crossing the country from west to east.

Acknowledgments, Samples, and Data

References

Abdu, M. A., I. S. Batista, P. Muralikrishna, J. H. A. Sobral (1996). Long term trends in sporadic E layers and electric fields over Fortaleza, Brazil. *Geophysical Research Letters*, 23(7), 757-760, doi:10.1029/96GL00589.

Abdu, M. A. (1997). Major phenomena of the equatorial ionosphere- thermosphere system under disturbed conditions. *Journal of Atmospheric and Terrestrial Physics*, 59, 1505-1519, doi:10.1016/S1364-6826(96)00152-6.

Abdu, M. A., J. R. de Souza, J. H. A. Sobral, and I. S. Batista (2006). Magnetic storm associated disturbance dynamo effects in the low and equatorial latitude ionosphere, in Recurrent Magnetic Storms: Corotating Solar Wind Streams. *Geophysical Monograph Series*, 167, 283-304, doi:10.1029/167GM22.

Abdu, M. A., Batista, I. S., Reinisch, B. W., de Souza, J. R., Sobral, J. H. A., Pedersen, T. R., Groves, K. M. (2009a). Conjugate Point Equatorial Experiment (COPEX) campaign in Brazil: Electrodynamics highlights on spread development conditions and day-to-day variability. *Journal of Geophysical Research: Space Physics*, 114(A4), 1-21. doi:10.1029/2008ja013749.

Abdu, M. A., G. M. Brum. (2009b). Electrodynamics of the vertical coupling processes in the atmosphere-ionosphere system of the low latitude region. *Earth, Planets Space*, 61, 385-395, doi: 10.1186/BF03353156.

Abdu, M. A., J. R. de Souza, I. S., Batista, M. A. Santos, J. H. A. Sobral, R. G. Rastogi, H. Chandra (2014). The role of electric fields in sporadic E layer formation over low latitudes under quiet and magnetic storm conditions. *Journal of Atmospheric and Terrestrial Physics*, 115, 95-105, doi: 10.1016/j.jastp.2013.12.003.

Balan, N., Alleyne, H., Walker, S., Reme, H., McCrea, I., Aylward, A. (2008). Magnetosphere-ionosphere coupling during the CME events of 07–12 November 2004. *Journal of Atmospheric and Terrestrial Physics*, 70(17), 2101–2111, doi:10.1016/j.jastp.2008.03.015

Batista, I. S., Abdu, M. A., Carrasco, A. J., Reinisch, B. W., de Paula, E. R., Schuch, N. J., Bertoni, F. (2008). Equatorial spread F and sporadic E-layer connections during the Brazilian Conjugate Point Equatorial Experiment (COPEX). *Journal of Atmospheric and Solar-Terrestrial Physics*, 70(8-9), 1133–1143, doi:10.1016/j.jastp.2008.01.007.

Batista, I. S., Candido, C. M. N., Souza, J. R., Abdu, M. A., de Araujo, R. C., Resende, L. C. A. Santos, A. M. (2017). F3 layer development during quiet and disturbed periods as observed at conjugate locations in Brazil: The role of the meridional wind. *Journal of Geophysical Research: Space Physics*, 122, 2361-2373, doi:10.1002/2016JA023724.

Bishop, R. L., Earcle, G. D. (2003). Metallic ion transport associated with midlatitude intermediate layer development. *Journal of Geophysical Research: Space Physics*, 108 (A1), 10-19. http:// dx.doi.org/10.1029/2002JA009411.

642 Blanc, M., Richmond, A. D. (1980). The ionospheric disturbance dynamo. *Journal of*
643   *Geophysical Research: Space Physics*, 85(A4), 1669–1686.
644   doi:10.1029/JA085iA04p01669.

645 Buriti, R. A., Hocking, W. K., Batista, P. P., Medeiros, A. F. (2008). Observations of equatorial
646   mesospheric winds over Cariri (7.4° S) by a meteor radar and comparison with existing
647   models. *Annales Geophysicae*, 26, 485-497, doi: 10.5194/angeo-26-485-2008.

648 Carrasco, A. J., Batista, I. S., Abdu M. A. (2007). Simulation of the sporadic E layer response to
649   pre-reversal associated evening vertical electric field enhancement near dip equator.
650   *Journal of Geophysical Research: Space Physics*, 112(A06):324-335,
651   doi:10.1029/2006JA012143.

652 Dagar, R., P. Verma, O. Napgal, C. S. G. K. Setty (1977), The relative effects of electric fields
653   and neutral winds on the formation of the equatorial sporadic layers. *Annales*
654   *Geophysicae*, 33(3), 333–340.

655 Da Silva, L. A., Satyamurty, P., Alves, L. R., Souza, V. M., Jauer, P. R., Silveira, M. V. D.,
656   Vieira, L. E. A. (2016). Comparison of geophysical patterns in the southern hemisphere
657   mid-latitude region. *Advances in Space Research*, 58(10), 2090–2103,
658   doi:10.1016/j.asr.2016.04.003.
659 Denardini, C. M., Dasso, S., Gonzalez-Esparza, J. A. (2016). Review on space weather in Latin America.
660   2. The research networks ready for space weather. *Advances in Space Research*, 58(10), 1940–1959.
661   https://doi.org/10.1016/j.asr.2016.03.013

662

663 Fürst, F., Wilms, J., Rothschild, R. E., Pottschmidt, K., Smith, D. M., and Lingenfelter, R.(2009).
664   Temporal variations of strength and location of the South Atlantic Anomaly as measured
665   by RXTE. *Earth Planet Science Letters*, 281, 125–133, doi:10.1016/j.epsl.2009.02.004.

666 Ginet, G. P., Madden, D., Dichter, B. K., and Brautigam G, D. H. (2007). Energetic proton maps
667   for the South Atlantic Anomaly. *IEEE Radiation Effects Data Workshop*, Honolulu, HI,
668   USA, 23–27 July 2007, 1–8.

669 Gonzalez, W.D., Joselyn, J.A., Kamide, Y., Kroehl, H.W., Rostoker, G., Tsurutani, B.T.,
670   Vasyliunas, V.M. (1994). What is a magnetic storm? *Journal of Geophysical Research:*
671   *Space Physics*, 99 (A4), 5771-5792, doi: doi.org/10.1029/93JA02867.

672 Hagan, M. E., Forbes, J. M. (2002). Migrating and nonmigrating diurnal tides in the middle and
673   upper atmosphere excited by tropospheric latent heat release. *Journal of Geophysical*
674   *Research: Space Physics*, 107(D24), 4754, doi:10.1029/2001JD001236.

675 Hagan, M. E., Forbes, J. M. (2003). Migrating and nonmigrating semidiurnal tides in the upper
676   atmosphere excited by tropospheric latent heat release. *Journal of Geophysical Research:*
677   *Space Physics*, 108(A2), 1062, doi:10.1029/2002JA009466.

678 Haldoupis, C., Meek, C., Christakis, N., Pancheva, D., Bourdillon, A. (2006). Ionogram height-
679   time intensity observations of descending sporadic E layers at mid-latitude. *Journal of*

Atmospheric and Terrestrial Physics, 68 (539), 539–557, doi:10.1016/
j.jastp.2005.03.020.

Haldoupis, C. (2011). A tutorial review on Sporadic E layers, Aeronomy of the Earth's
Atmosphere-Ionosphere. *IAGA Book Series*, 29 (2), 381-394, doi: 10.1007/978-94-007-
0326-1_29.

Hedin, A. E., Biondi, M. A., Burnside, R. G., Hernadez, G., Johson, R. M., Killen, T. L.,
Mazaudier, C., Meriwether, J. W., Salah, J. E., Sica, R. J., Smith, R. W., Spencer, N. W.,
Wickwar, V. B., Virdi, T. S. (1991). Revised global model of thermosphere winds using a
satellite and ground-based observations. *Journal of Geophysical Research: Space
Physics*, 96(A5), 7657–7688, doi: 10.1029/91JA00251.

Fejer, B. G., Scherliess,L. (1995). Time dependent response of equatorial ionospheric electric
fields to magnetospheric disturbances. *Geophysical Research Letters*, 22, 851-854, doi:
10.1029/95gl00390.

Fejer, B. G. (1997). The electrodynamics of the low-latitude ionosphere: Recent results and
future challenges. *Journal of Atmospheric and Terrestrial Physics*, 59, 1465–1482, doi:
10.1016/S1364-6826(96)00149-6.

Fejer B. G., Jensen J. W., Su S. Y. (2008). Seasonal and longitudinal dependence of equatorial
disturbance vertical plasma drifts *Geophysical Research Letters*, 35(L20106):2008G,
doi:10.1029/L035584.

Kelley, M. C., Makela, J. J., Chau, J. L., Nicolls, M. J. (2003), Penetration of the solar wind
electric field into the magnetosphere/ionosphere system. *Geophysical Research Letter*,
30(4), 1158, doi:10.1029/2002GL016321.

Kennel, C. F. and H. E. Petschek. (1966). Limit on stably trapped particle fluxes. Journal
Geophys. Reseach. https://doi.org/10.1029/JZ071i001p00001

Kopp, E. (1997), On the abundance of metal ions in the lower ionosphere. *Journal of
Geophysical Research: Space Physics*, 102, 9667- 9674, doi: 0148-0227/97/97JA-
003845.

Mauk, B. H., N. J. Fox, S. G. Kanekal, R. L. Kessel, D. G. Sibeck, and A. Ukhorskiy. (2012).
Science objectives and rationale for the radiation belt storm probes mission. *Space
Science Review*, 179, 3–27, doi:10.1007/s11214-012-9908-y.

Mathews, J. D. (1998). Sporadic E: current views and recent progress. *Journal of Atmospheric
and Terrestrial Physics*, 60, 413-435, doi: 10.1016/S1364-6826(97)00043-6.

Moro, J., L. C. A. Resende, C. M. Denardini, J. Xu, I. S. Batista, V. F. Andrioli, N. J. Schuch,
(2017). Equatorial E region electric fields and sporadic E layer responses to the recovery
phase of the November 2004 geomagnetic storm. *Journal of Geophysical Research:
Space Physics*, 122, 12,517–12,533. https://doi.org/10.1002/2017JA024734.

Nogueira, P.A.B.; Abdu, M.A ; Batista, I. S.; Siqueira, P.M. (2011). Equatorial ionization
anomaly and thermospheric meridional winds during two major storms over Brazilian

low latitudes. *Journal of Atmospheric and Solar-Terrestrial Physics*, v. 73, p. 1535-1543, doi: 10.1016/j.jastp.2011.02.008.

Otsuka, Y., T. Ogawa, A. Saito, T. Tsugawa, S. Fukao, and S. Miyazaki (2002), A new technique for mapping of total electron content using GPS network in Japan. *Earth Planets Space*, 54, 63-70, doi:10.1186/BF03352422

Pignalberi, A., M. Pezzopane, E. Zuccheretti (2014). Sporadic E layer at mid-latitudes: average properties and influence of atmospheric tides. *Annales Geophysicae*, 32, 1427-1440, doi: 0.5194/angeo-32-1427-2014.

Prasad, S. N. V. S., D. S. V. V. D. Prasad, K. K. Venkatesh, K. Niranjan, P. V. S. Rama Rao (2012). Diurnal and seasonal variations in sporadic E-layer (Es layer) occurrences over equatorial, low and mid latitude stations - A comparative study. *Indian Journal Radio Space Physics*, 41, 26-35.

Reddy, C. A. and M.M. Rao (1968). On the physical significance of the Es parameters *fb*Es, *ft*Es and *fo*Es. *Journal of Geophysical Research: Space Physics*, 21, 3, 331-341, doi: 10.1029/JA073i017p05627.

Reinisch, B.W., Galkin, I.A., Khmyrov, G.M., et al., 2009. The new Digisonde for research and monitoring applications. *Radio Science*, 44, doi: 10.1029/2008RS004115.

Resende, L. C. A., I. S. Batista, C. M. Denardini, A. J. Carrasco, V. F. Andrioli, J. Moro, P. P. Batista, S. S. Chen (2016), Competition between winds and electric fields in the formation of blanketing sporadic E layers at equatorial regions. *Earth Planets and Space*, 68:201, doi:10.1186/s40623-016-0577-z.

Resende, L. C. A., I. S. Batista, C. M. Denardini, P. P. Batista, A. J. Carrasco, V. F. Andrioli, J. Moro (2017a), Simulations of blanketing sporadic E-layer over the Brazilian sector driven by tidal winds. *Journal of Atmospheric and Solar-Terrestrial Physics*, 154, 104-114, doi:10.1016/j.jastp.2016.12.012.

Resende, L. C. A., I. S. Batista, C. M. Denardini, P. P. Batista, J. A. Carrasco, V. F. Andrioli, J. Moro (2017b). The influence of tidal winds in the formation of blanketing sporadic E-layer over equatorial Brazilian region. *Journal of Atmospheric and Solar-Terrestrial Physics*, 171, 64-67, doi:10.1016/j.jastp.2017.06.009.

Rishbeth, H., Ganguly, S., Walker, J. C. G. (1978). Field-aligned and field-perpendicular velocities in ionospheric F2-layer. *Journal of Atmospheric and Solar-Terrestrial Physics*, 40, 7, 767-784, doi: 10.1016/0021-9169(78)90028-4.

Santos, A., M., Abdu, M.A., Sobral, J. H., Koga, D., Nogueira, P. A. B., Candido, C. M. N. (2012). Strong longitudinal difference in ionospheric responsesover Fortaleza (Brazil) and Jicamarca (Peru) during the January 2005 magnetic storm, dominated by northward IMF. *Journal of Geophysical Research: Space Physics*, 117,A0833,1-10, doi: 10.1029/2012JA017604.

Santos, A., M., Abdu, M.A ; Souza, J. R., Sobral, J. H., Batista, I. S.; Denardini, C. M. (2016). Stormtime equatorial plasma bubble zonal drift reversal due to disturbance Hall electric

757   field over the Brazilian region: Disturbed zonal plasma drift. *Journal of Geophysical*
758   *Research: Space Physics*, 121, 6,1-19, doi:10.1002/2015JA022179.

759 Sastri, J. H. (1988), Equatorial electric fields of ionospheric disturbance dynamo origin. *Annales*
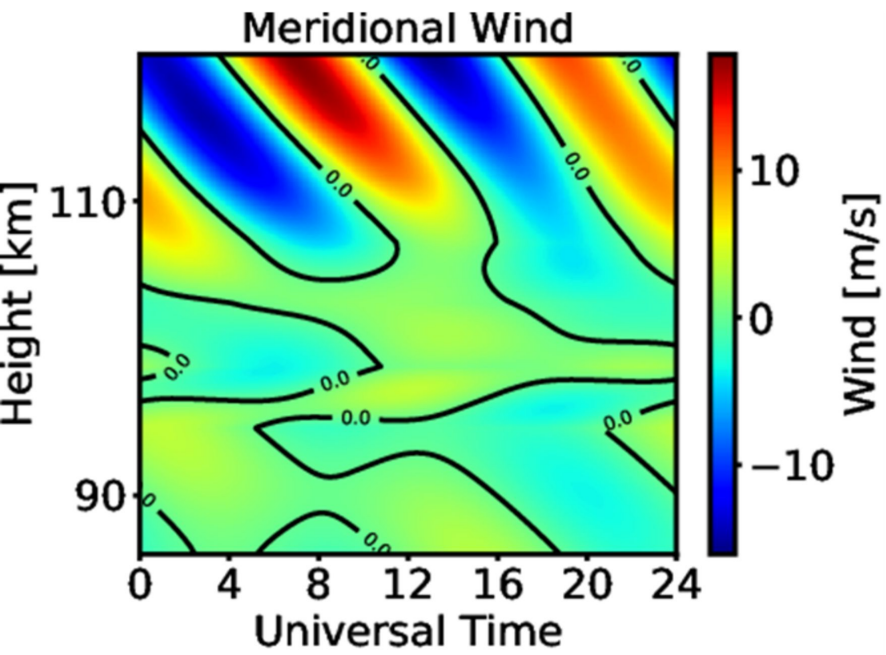760   *Geophysicae*, 6, 635-642.

761 Takahashi, H., Wrasse, C. M, Denardini, C. M., Pádua, M. B., de Paula, E. R., Costa, S.M. A.,
762   Otsuka, Y., Shiokawa, K., Galera Monico, J. F., Ivo, A., N. Sant'Anna, N. (2016).
763   Ionospheric TEC Weather Map Over South America. *Space Weather*, 14, 937–949,
764   doi:10.1002/2016SW001474

765 Thorne, R. M. (2010). Radiation belt dynamics: The importance of wave-particle interactions,
766   *Geophysical Research Letters*. 37, L22107, doi:10.1029/2010GL044990.

767 Whitehead, J. (1961). The formation of the sporadic-E in the temperate zones. *Journal of*
768   *Atmospheric and Terrestrial Physics*, 20,1, 1155-1167, doi: 10.1016/0021-
769   9169(61)90097-6.

Figure 1.

a) Meridional Wind

b) Zonal Wind

Figure 2.

a

b

c

d
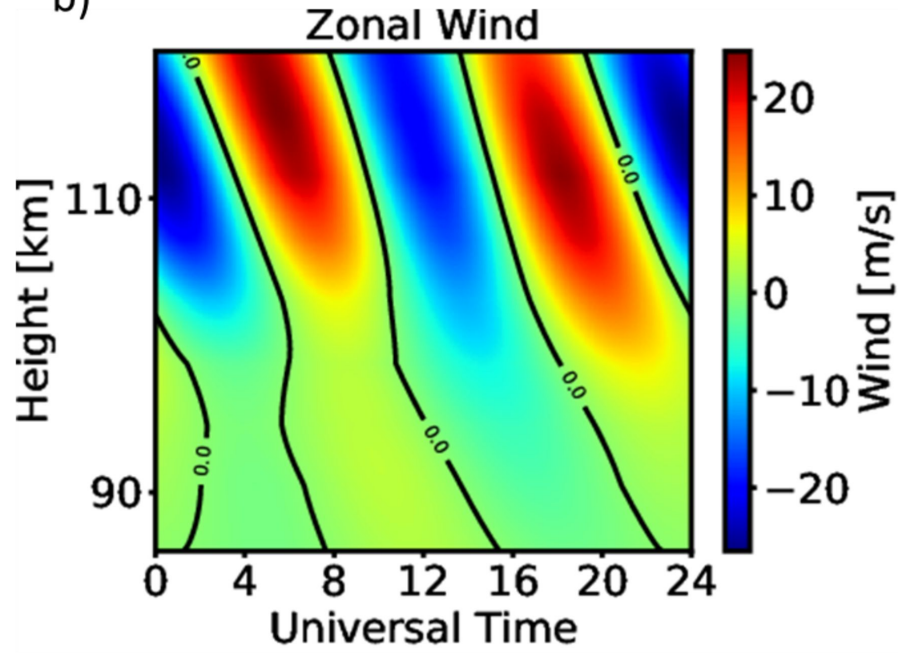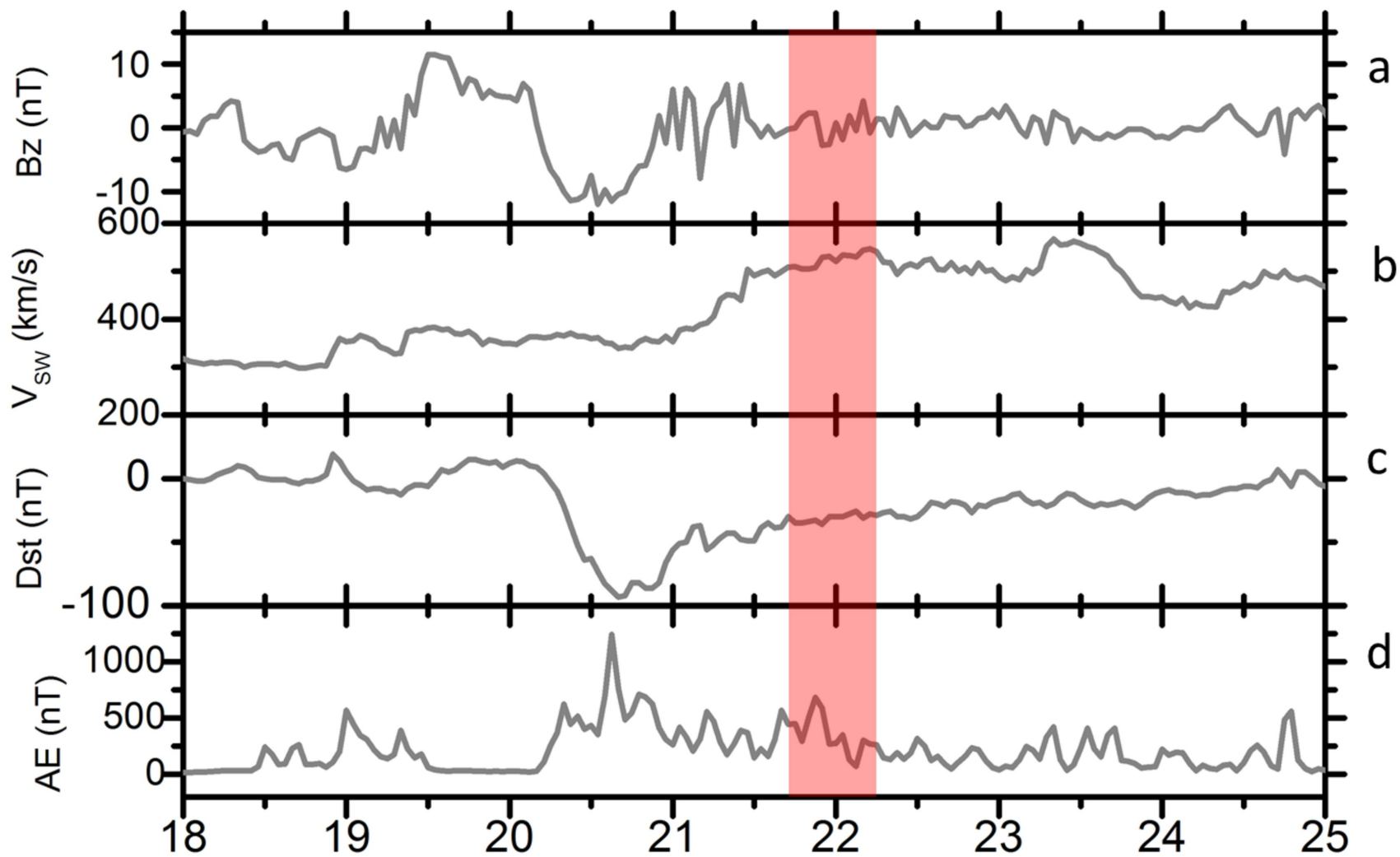
January, 18-25, 2016

Figure 3.

Figure 4.

Figure showing fbEs/ftEs ratios for four stations (a) BV, (b) CG, (c) FLZ, (d) SLZ over January, 21-23, 2016. Orange line: ftEs; green line: fbEs.
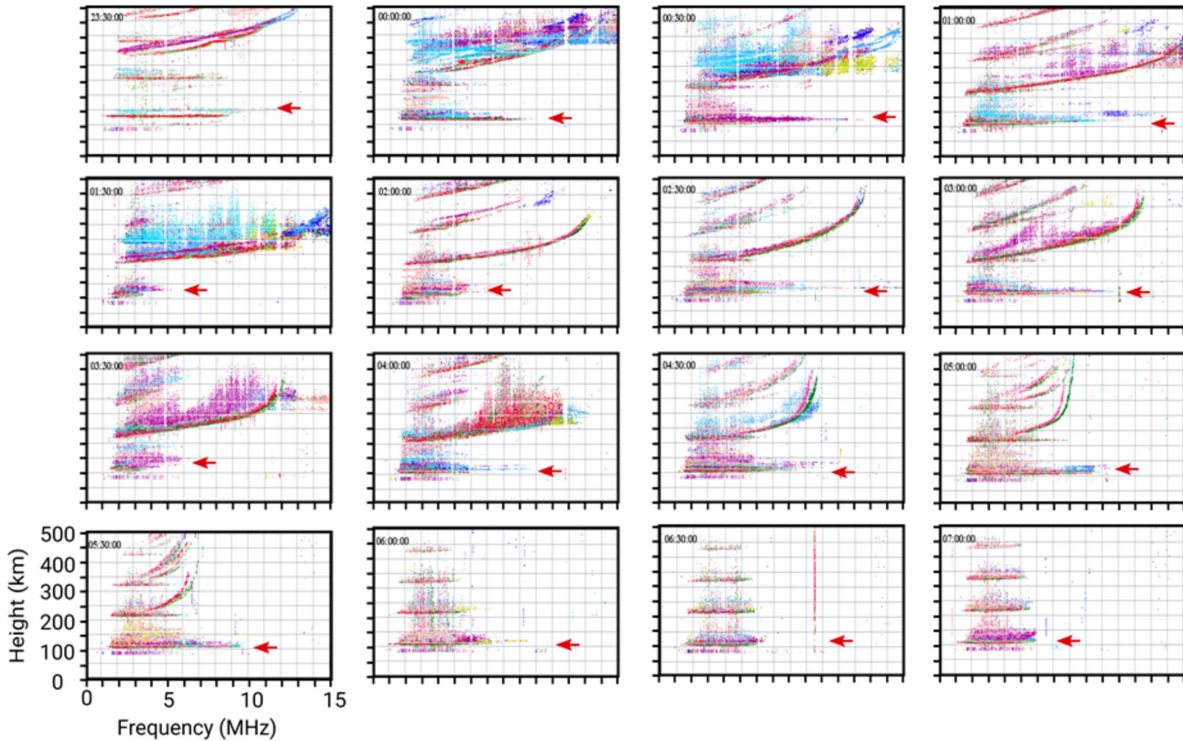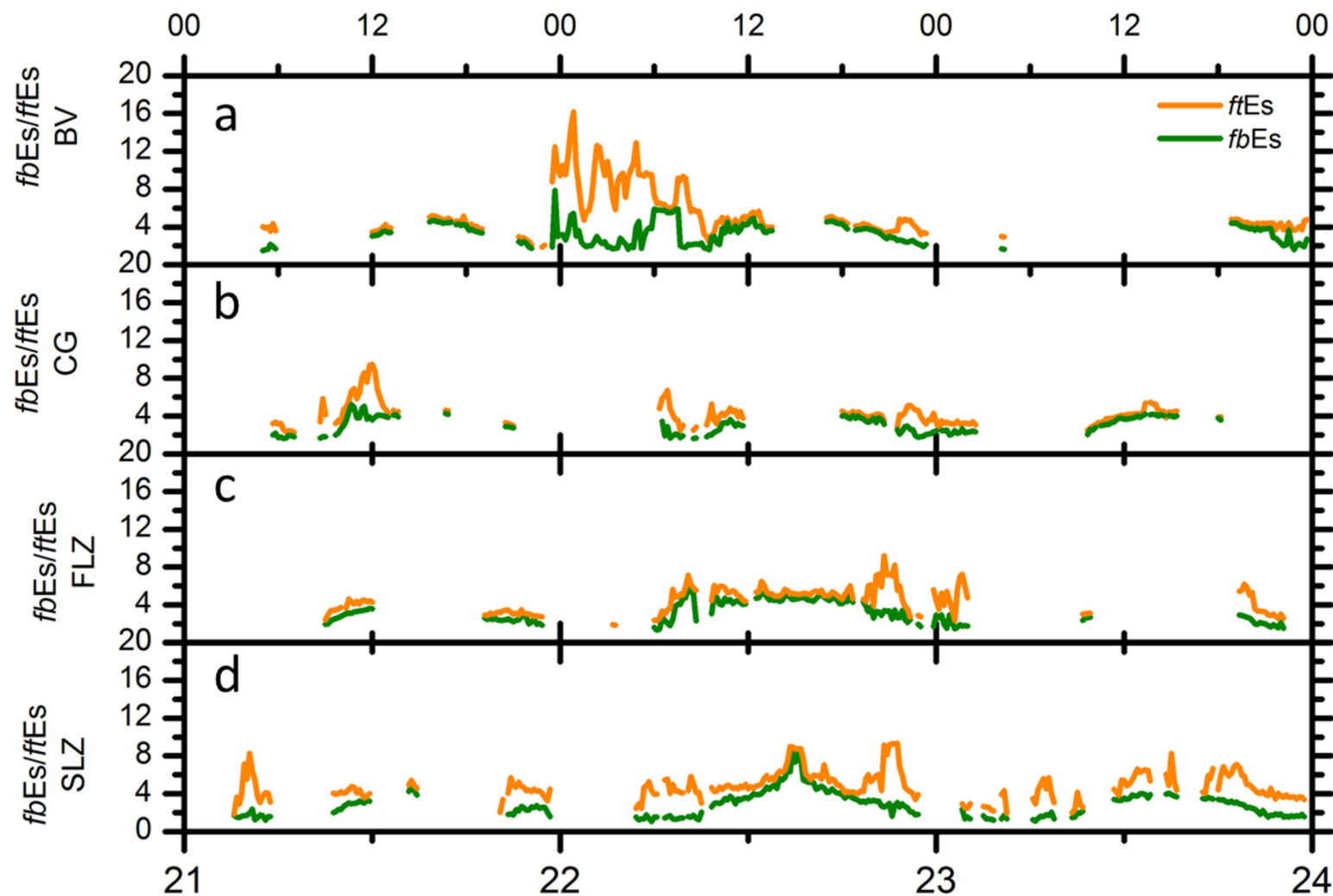
Figure 5.

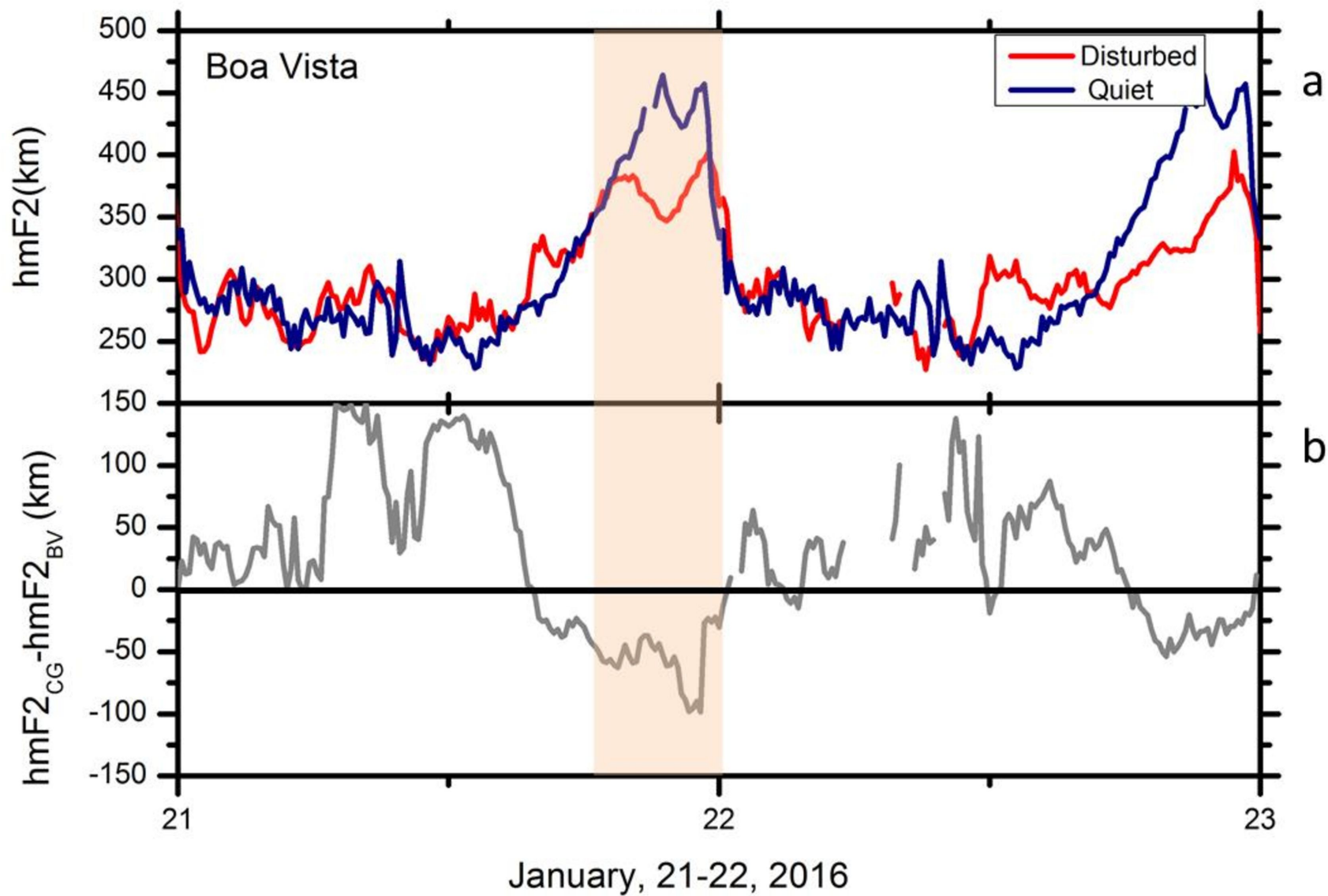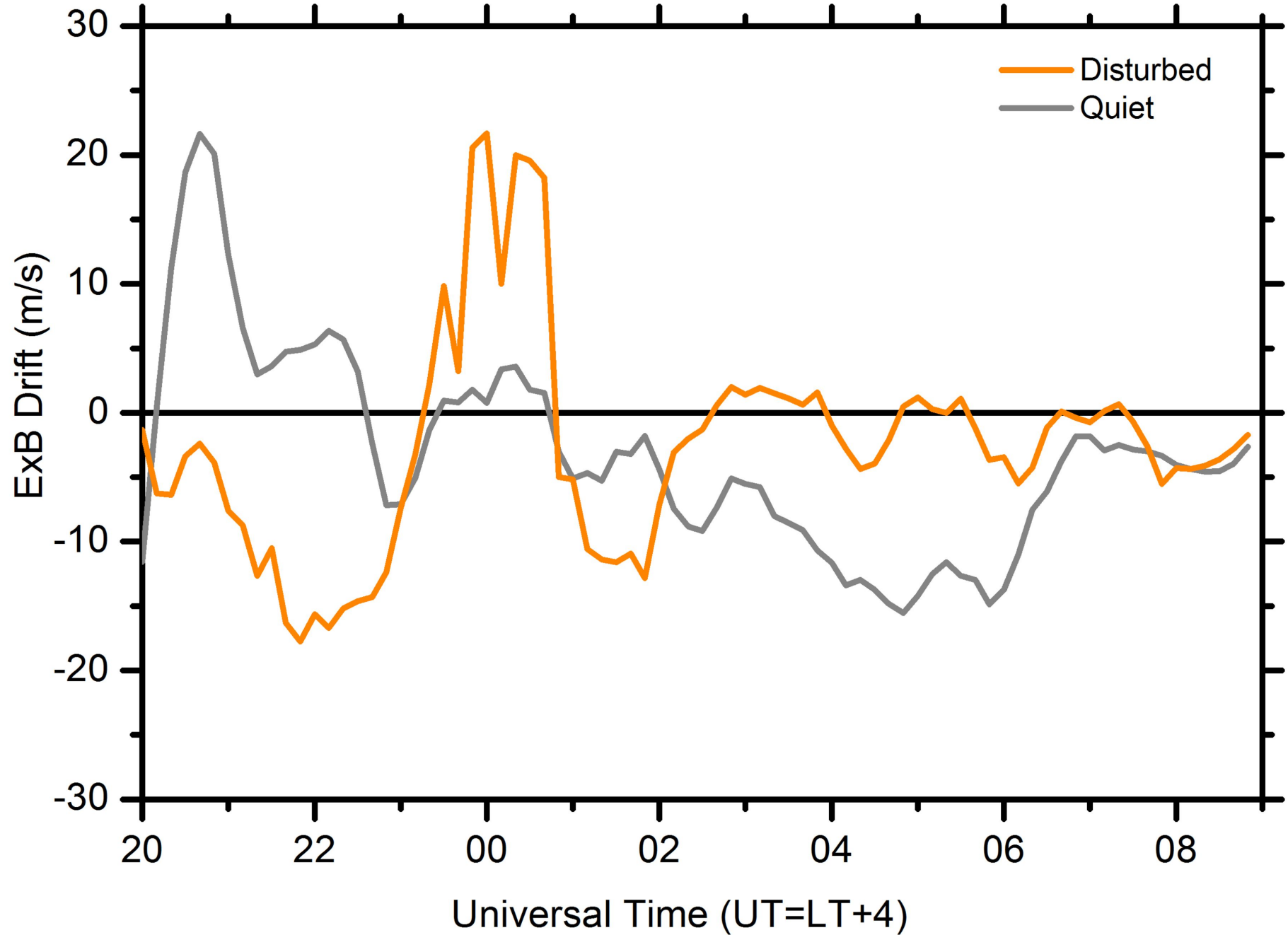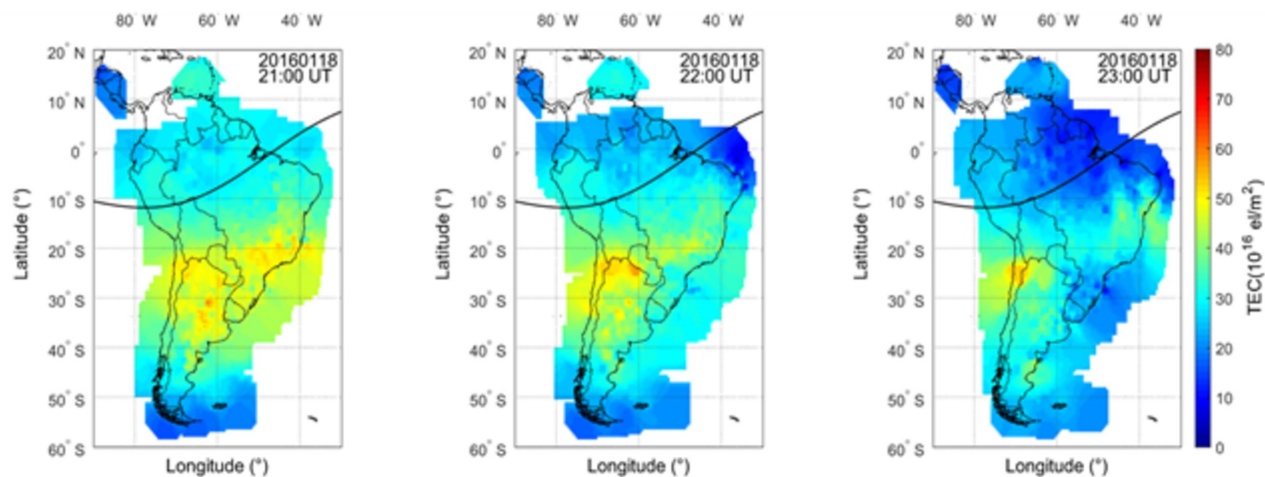**Figure 6.**

January, 21-22, 2016

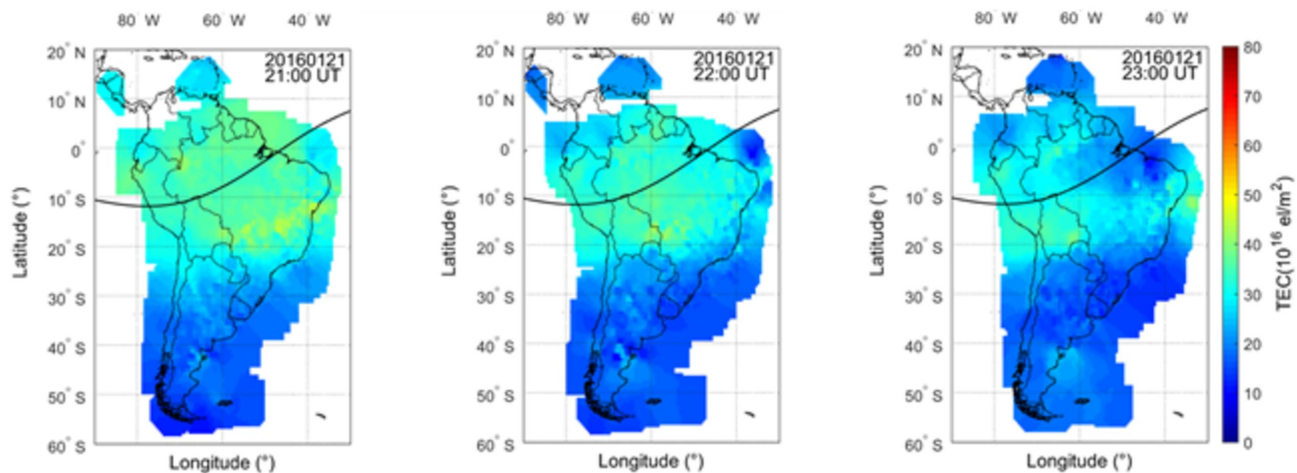**Figure 7.**

January, 18, 2016
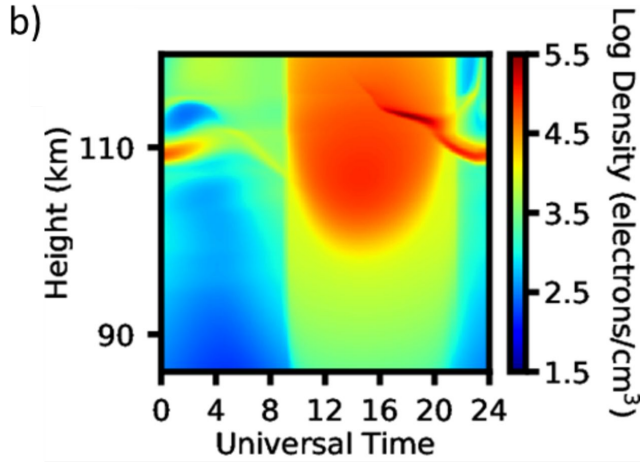
a)

January, 21, 2016

b)

Figure 8.

Figure 9.

a)

b) Log Density (electrons/cm³)